Liquid Crystals
Publication details, including instructions for authors and subscription information:
http://www.informaworld.com/smpp/title~content=t713926090

Synthesis and liquid crystal properties of a new class of calamitic mesogens based on substituted 2,5-diaryl-1,3,4-thiadiazole derivatives with wide mesomorphic temperature ranges

Jie Han[a]; Xiao-Yong Chang[a]; Li-Rong Zhu[a]; Yan-Mei Wang[a]; Ji-Ben Meng[a]; Siu-Wai Lai[b]; Stephen Sin-Yin Chui[b]
[a] Department of Chemistry, Nankai University, Tianjin, P. R. China [b] Department of Chemistry and HKU-CAS Joint Laboratory on New Materials, The University of Hong Kong, Hong Kong, P. R. China

Online publication date: 06 July 2010

To cite this Article Han, Jie , Chang, Xiao-Yong , Zhu, Li-Rong , Wang, Yan-Mei , Meng, Ji-Ben , Lai, Siu-Wai and Chui, Stephen Sin-Yin(2008) 'Synthesis and liquid crystal properties of a new class of calamitic mesogens based on substituted 2,5-diaryl-1,3,4-thiadiazole derivatives with wide mesomorphic temperature ranges', Liquid Crystals, 35: 12, 1379 — 1394
To link to this Article: DOI: 10.1080/02678290802617724
URL: http://dx.doi.org/10.1080/02678290802617724

Liquid Crystals,
Vol. 35, No. 12, December 2008, 1379–1394

Taylor & Francis
Taylor & Francis Group

Synthesis and liquid crystal properties of a new class of calamitic mesogens based on substituted 2,5-diaryl-1,3,4-thiadiazole derivatives with wide mesomorphic temperature ranges

Jie Han[a]*, Xiao-Yong Chang[a], Li-Rong Zhu[a], Yan-Mei Wang[a], Ji-Ben Meng[a], Siu-Wai Lai[b] and Stephen Sin-Yin Chui[b]**

[a]*Department of Chemistry, Nankai University, Tianjin, P. R. China;* [b]*Department of Chemistry and HKU-CAS Joint Laboratory on New Materials, The University of Hong Kong, Pokfulam Road, Hong Kong, P. R. China*

(Received 2 September 2008; in final form 12 November 2008)

Liquid crystals based on substituted 2,5-diaryl-1,3,4-thiadiazole derivatives (**1a**–**1f**, **3a** and 3b) and 1,3,4-oxadiazole analogues (**2a**–**2f**, **4a** and **4b**) were synthesised and characterised by ^{1}H, ^{13}C nuclear magnetic resonance, Fourier transform infrared, mass spectrometry, high-resolution mass spectrometry techniques and elemental analyses. The X-ray crystal structure of **1e** revealed that it contains tilted lamellar arrangement of molecules in the crystalline solid. The liquid crystal properties have been investigated by polarised-light optical microscopy, differential scanning calorimetry and *in-situ* variable-temperature X-ray diffraction. All compounds (except **2e** and **2f**) exhibited thermotropic liquid crystal behaviours with various mesophases (smectic A and C, nematic N or soft crystal E phases). Notably, the 1,3,4-thiadiazole derivatives consistently have wider mesomorphic temperature ranges than those of the respective 1,3,4-oxadiazole analogues. The solutions of all compounds in CH_2Cl_2 individually displayed one or two absorption bands with λ_{max} values at 297–355 nm and emitted with λ_{max} values at 363–545 nm and quantum yields of 0.12–0.73. Structure–property relationships of these compounds are discussed in the contexts of their molecular structures and weak intermolecular interactions.

Keywords: heterocyclic liquid crystals; phase transition; microwave-assisted synthesis; structure-property relationship

1. Introduction

Rational design and synthesis of π-conjugated mesogenic molecules is an important research interest in the fields of physics, chemistry, materials science and engineering because these low-molecular-weight materials could be readily modified and exhibit interesting electronic, luminescent and liquid crystal properties, which favours the development of new functional materials in liquid crystal display, electronic and optoelectronic applications (*1–6*). In the literature, there is considerable interest regarding mesogenic materials adopting either rod-like (calamitic) or disc-like (discotic) molecular shapes. Liquid crystals of both shape types based on substituted 2,5-diaryl-1,3,4-oxadiazole derivatives have been extensively studied due to their good thermal and chemical stability, photoluminescence quantum yields and the electron-deficient feature of the 1,3,4-oxadiazole ring (*7–19*). Regarding material stability and processibility, exploration of structurally robust liquid crystals with wide mesomorphic temperature ranges and good photoluminescence quantum yields is one of crucial steps for development of high-performance optoelectronic and electroluminescent devices using polarised-light emission (*5, 6*). However, most of the as-formed mesophases from 1,3,4-oxadiazole derivatives briefly exist in a relatively narrow temperature range ΔT (that is defined by the difference between melting T_m and clearing temperatures T_c), which inevitably limits the mesomorphic stability for practical uses. In this regard, Watanabe and Dinggemans groups reported different types of symmetric 1,3,4-oxadiazole derivatives containing biphenyl spacers and ester linkages, which produced mesophases with moderate mesomorphic temperature ranges of 191–261°C (*13*) and 148–222°C, respectively (15). Lai et al. reported some disc-like Pd(II)-metallomesogen with dichlorobis 2,5-bis (3,4,5-trimethoxy phenyl)-1,3,4-oxadiazole ligand that produced interesting columnar mesophases with a wide mesomorphic temperature range up to 126°C (*12*). It is noteworthy to point out that related study on liquid crystals based on 2,5-diaryl-1,3,4-thiadiazole is relatively scarce (*20–28*). Herein, we report a class of calamitic mesogenic materials based on substituted 2,5-diaryl-1,3,4-thiadiazole derivatives formulated as [*p*-$C_{10}H_{21}O$-C_6H_4-(SC_2N_2)-(*p*-C_6H_4)$_n$-*R*] (where *p*-C_6H_4 and SC_2N_2 represent a *p*-phenylene spacer, 1,3,4-thiadiazole ring, respectively

Corresponding authors. *Email: hanjie@nankai.edu.cn; **chuissy@hkucc.hku.hk

ISSN 0267-8292 print/ISSN 1366-5855 online

DOI: 10.1080/02678290802617724
http://www.informaworld.com

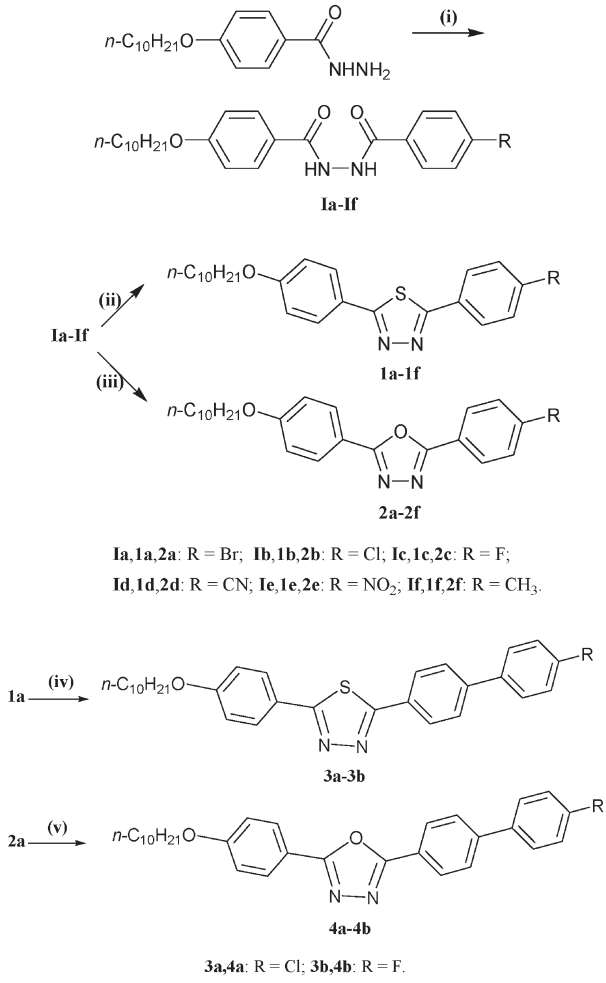

Figure 1. Synthesis of **1a**–**1f**, **2a**–**2f**, **3a**–**3b** and **4a**–**4b**. (i) *para*-substituted benzoyl chlorides, 70°C, 1 h, 70–80%; (ii) Lawesson's reagent, microwave irradiation: 2–4 min, 45–75%; (iii) $SOCl_2$, reflux, 7 h, 75–85%; (iv) *para*-substituted benzyl boronic acids, $KF{\cdot}2H_2O$, and $Pd(OAc)_2$, microwave irradiation: 30 s, 39–48%; (v) *para*-substituted benzyl boronic acids, K_2CO_3, $Pd(OAc)_2$, H_2O, dioxane, reflux, 1 h, 83–90%.

and substituent R=Br, Cl, F, CN, NO_2, and CH_3). The synthetic routes of all these compounds used in this work are shown in Figure 1. All 1,3,4-thiadiazole derivatives formed a variety of liquid crystal phases, as confirmed by polarised-light optical microscopy (POM), differential scanning calorimetry (DSC) and in-situ variable-temperature X-ray diffraction (VTXRD) studies. Changing (i) the heteroatom (X=S and O) of the XC_2N_2 heterocyclic ring, (ii) the terminal substituents and (iii) the number of *p*-phenylene spacer (n=1, 2) of molecules significantly alters their mesomorphic and photoluminescent properties. Notably, compared with 1,3,4-oxadiazole analogues, all mesophases derived from 1,3,4-thiadiazole derivatives have wider mesomorphic temperature ranges.

2. Results

2.1 Synthesis and characterisation

The 1,3,4-thiadiazole derivatives were prepared by the sulphuration reaction of 1,4-dicarbonyl precursors with P_2S_5 and Lawesson's reagent in anhydrous hydrocarbon solvents at high temperature (*29, 30*). In addition, microwave-assisted reaction conditions were used due to their low cost, operational simplicity and effectiveness as well as high product yields, requiring relatively shorter reaction time (*31, 32*). The 1,3,4-thiadiazole derivatives **1a**–**1f** were obtained in moderate to good yields (45–75%) by using this kind of synthetic strategy, which was carried out under solvent-free and microwave irradiation conditions (*33–35*), while the 1,3,4-oxadiazole analogues **2a**–**2f** were prepared by using methods modified from the literature (*36*). The most common method involved refluxing *N,N′*-diacylhydrazines in an anhydrous benzene solution containing either thionyl chloride (*36*), polyphosphoric acid (*37*), phosphorus oxychloride (*38*), or polymer-supported PPh_3/CCl_3CN (*39*). We found that **2a**–**2f** were prepared in good yields (75–85%) by refluxing the reaction mixture with thionyl chloride. The 1,3,4-oxadiazoles **4a**–**4b** were obtained in high yields (83–90%) via the Suzuki cross-coupling reaction (*41*). However, preparation of the 1,3,4-thiadiazoles **3a**–**3b** using similar reaction conditions was unsuccessful, even though different catalytic conditions such as $Pd(PPh_3)_4/K_2CO_3$/dioxane-H_2O (*41*) $PdCl_2/K_2CO_3$/pyridine (*42*), and $Pd(OAc)_2/Na_2CO_3/H_2O$-PEG (*43*) were employed. We subsequently realised that the poor solubility of reactants under these conditions and the coordination of the sulphur atom of the thiadiazole to the Pd-catalyst might be the reason why these reactions failed. Finally **3a**–**3b** were obtained by using the literature method with slight modifications (*44*). For instance, we found that the solvent-free reactions using KF-$2H_2O$ rather than KF-Al_2O_3 under short microwave irradiation could significantly increase the yields (39–48%) of the products.

2.2 X-ray crystal structure of 1e

Slow evaporation of CH_2Cl_2 solution of **1e** at room temperature afforded yellow plate-like crystals suitable for single crystal X-ray diffraction determination; the crystallographic data are summarised in the Notes section. Figure 2 depicts the molecular structure of **1e** and the packing of molecules viewed from

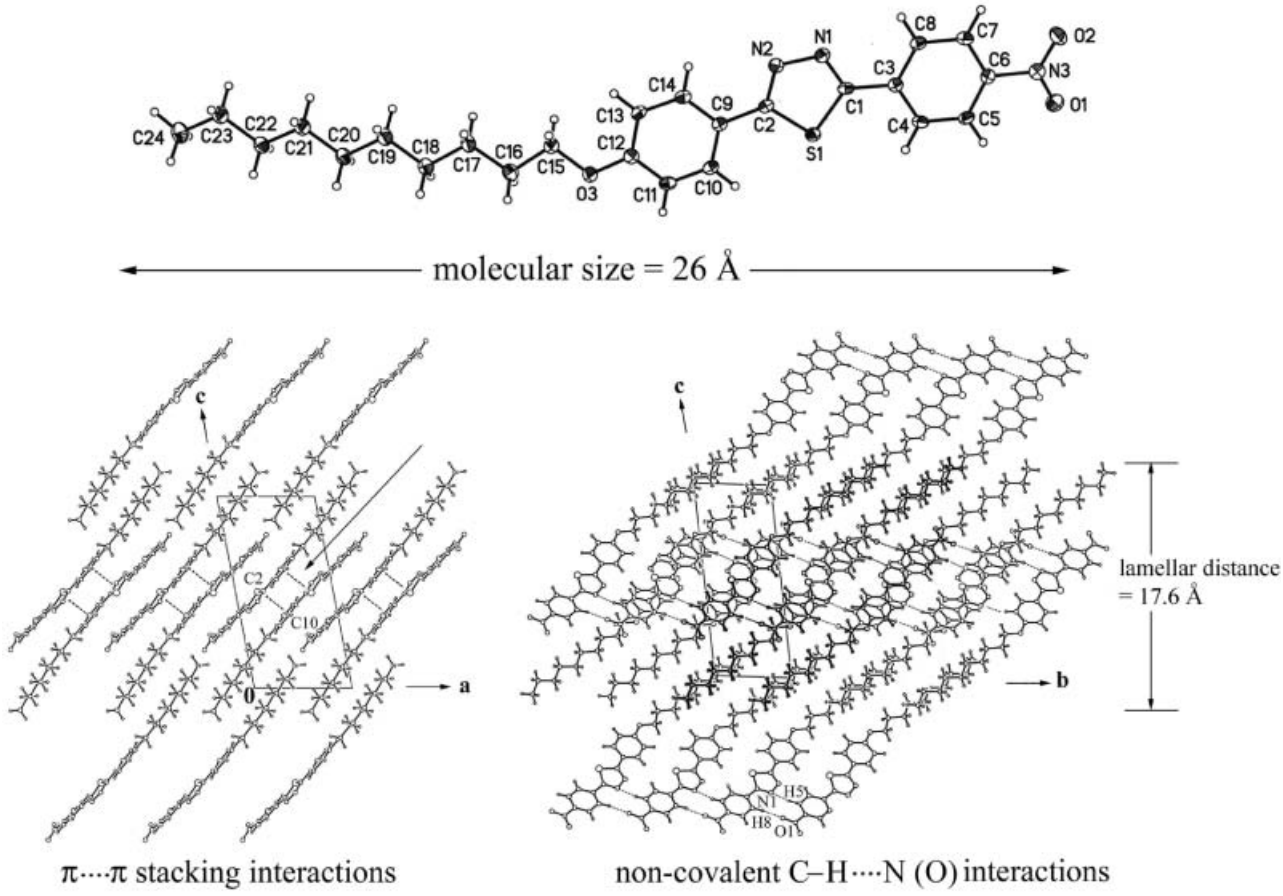

Figure 2. 50% ORTEP diagram of **1e** (top) and tilted lamellar arrangement of molecules viewed along the [100] and [010] direction of the crystal lattice (bottom). Note that π···π stacking and C–H···O(N) interactions are highlighted with dotted lines.

the [100] and [010] directions of the crystal lattice. The rod-shaped molecule of **1e** has an approximate size of 26 Å and its thiadiazole ring is roughly co-planar with the mean planes of the two attached *p*-phenylene rings. The NO_2 substituent is slightly twisted, which forms a dihedral angle (O1–N3–C5–C6) of 8.74° measured from the mean plane of the attached *p*-phenylene ring. Neighbouring pairs of molecules are aligned in an anti-parallel orientation by π···π stacking interactions (3.352 Å) between the thiadiazole carbon atom (C2) of one molecule and the other (C10) of the phenylene ring of its neighbor. Each molecule is laterally held by two types of non-covalent C–H···N(O) hydrogen bonding interactions between the hydrogen atoms (H5) of the phenylene ring and the nitrogen atoms (N1) of the thiadiazole ring ($d_{H\cdots N}$=2.499 Å), as well as the hydrogen atom (H8) and the oxygen atom (O1) of the NO_2 substituent ($d_{H\cdots O}$=2.574 Å). The terminal *n*-decyl chains of the molecules are packed together through inter-digitated hydroprobic interactions, leading to a repeating lamellar distance of 17.6 Å.

In addition, the comparison of C–S and C–N and N–N bond distances and angles of the heterocyclic rings of **1e**, the known compounds 2,5-diphenyl-1,3,4-thiadiazole (*45*) and 2,5-diphenyl-1,3,4-oxadiazole (*46*) has been made and the results are summarised in Table 1. We found that these geometric data of **1e** are consistent with that of 2,5-diphenyl-1,3,4-thiadiazole (*45*). The heteroatoms in the five-membered ring of all three cases were preferentially co-planar with the carbon and nitrogen atoms to form a planar π-conjugation system. Notably, the C–S–C angle (87.1°) of the 1,3,4-thiadiazole ring in **1e** is remarkably smaller than the C–O–C angle (103°) of 2,5-diphenyl-1,3,4-oxadiazole (*46*). The difference in C–*X* distances and C–*X*–C angles between thiadiazole and oxadiazole rings clearly accounts for the observation that molecule of **1e** adopts a rod-like conformation with large bend angles (167–169°) formed by intersecting the two adjacent C–C bonds at the centre of thiadiazole ring, compared with that of 136° of 2,5-diphenyl-1,3,4-oxadiazole.

Table 1. Selected bond distances and angles of heterocyclic rings in **1e**, 2,5-diphenyl-1,3,4-thiadiazole and 2,5-diphenyl-1,3,4-oxadiazole.

[XN_2C_2] heterocyclic ring

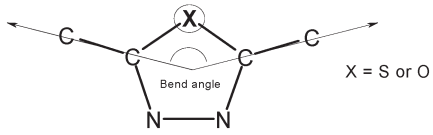

	1e	2,5,-diphenyl-1,3,4-thiadiazole[13]	2,5-diphenyl-1,3,4-oxadiazole[14]
C–*X* distances/Å	1.730, 1.734	1.759	1.376, 1.360
C–N distances/Å	1.312, 1.310	1.269	1.302, 1.296
N–N distances/Å	1.371	1.190	1.410
C–*X*–C angles/°	87.50	83.1	103.4
X–C–N angles/°	113.1, 113.4	111.6	112.1, 111.6
C–N–N angles/°	113.1, 112.9	116.7	106.2, 106.7
Bend angle/°	168	165	136

2.3 Electronic absorption and emission spectroscopy

The UV/Vis electronic absorption and emission data for the solutions of **1c**–**1f**, **2c**, and **3b** in CH_2Cl_2 at 298 K are listed in Table 2. For **1c**, and **1f**, each of them displayed a strong absorption band with a λ_{max} value at 324–329 nm (ε=31200–35100 $dm^3\,mol^{-1}\,cm^{-1}$) whereas **1d** and **1e** had two absorption bands (λ_{max} values=264 nm and 339 nm in **1d** and 278 nm and 355 nm in **1e**). The λ_{max} values of the low-energy absorption bands in **1c**–**1f** were progressively red-shifted from 324 nm to 355 nm when the electron-withdrawing ability of the substituents increased (CH_3 (**1f**), F (**1c**)<CN (**1d**)<NO_2 (**1e**)). This red-shift could be attributed to the electron-withdrawing substituent that lowered the lowest unoccupied molecular orbital energy level of the π-conjugation of the molecule. Unlike **1c**, the 1,3,4-oxadiazole analogue **2c** showed two absorption bands with λ_{max} values at 246 nm and 297 nm. In addition, when a *p*-phenylene spacer is inserted between the 1,3,4-thiadiazole and *p*-fluorophenyl units of **1c**, the energy of the absorption band was apparently lowered by 823 cm^{-1}, as revealed by the absorption band with a λ_{max} value of 335 nm (ε=45100 $dm^3\,mol^{-1}\,cm^{-1}$) in **3b**. All compounds in the CH_2Cl_2 solution were emissive with λ_{em} at 363–545 nm at room temperature. Notably, the poorer quantum yield of **1e** may be attributed to the intraligand n→π* excitation of the NO_2 substituent that suppressed the fluorescence signal from π→π* transition (*18*). **1e** also showed the largest Stokes shift of 9821 cm^{-1}, compared with that (5458–6188 cm^{-1}) of other 1,3,4-thaidiazole and 1,3,4-oxadiazole derivatives used in this work.

Table 2. UV/Vis electronic absorption and emission data for **1c**–**1f**, **2c** and **3b** in CH_2Cl_2 solution at 298 K.

Entry	λ_{abs}[nm] (ε[$dm^3mol^{-1}cm^{-1}$])	λ_{em} [nm][a]	Φ
1c	326 (31600)	405	0.31
1d	264 (sh, 11100), 339 (30500)	429	0.60
1e	278 (sh, 14100), 355 (24400)	545	0.12
1f	324 (31200)	398	0.26
2c	246 (sh, 7170), 297 (27500)	363	0.73
3b	335 (45100)	412	0.55

[a] λ_{ex} at λ_{max} absorption, at concentration=5×10^{-6} M.

2.4 Liquid crystal properties

The liquid crystal properties of all compounds were studied by POM and DSC. Except for the cases of **2e** and **2f**, all compounds exhibited thermotropic liquid crystal behaviours. Selected POM images of the mesophases obtained by heating the crystalline solid samples of **1c**, **1e**, **1f**, and **2a** or cooling their isotropic liquids are collectively depicted in Figure 3. The mesophases were identified according to the classification system reported by Kumar (*47*) and Dierking (*48, 49*). The phase transition temperatures (melting T_m and clearing T_c temperatures) and associated enthalpy changes derived from DSC measurements are listed in Table 3.

2.5 Powder X-ray diffraction

The powder X-ray diffraction (PXRD) patterns of all soli samples were recorded and the 2θ values and relative intensity of the strongest or three consecutive low-angle diffraction peaks are given in the Supporting Information which is available via the multimedia link on the online article webpage (Table S1). All solid samples were polycrystalline and free of any known impurities, derived from known starting materials or inorganic salts used in material syntheses. In most cases, the 2θ values of

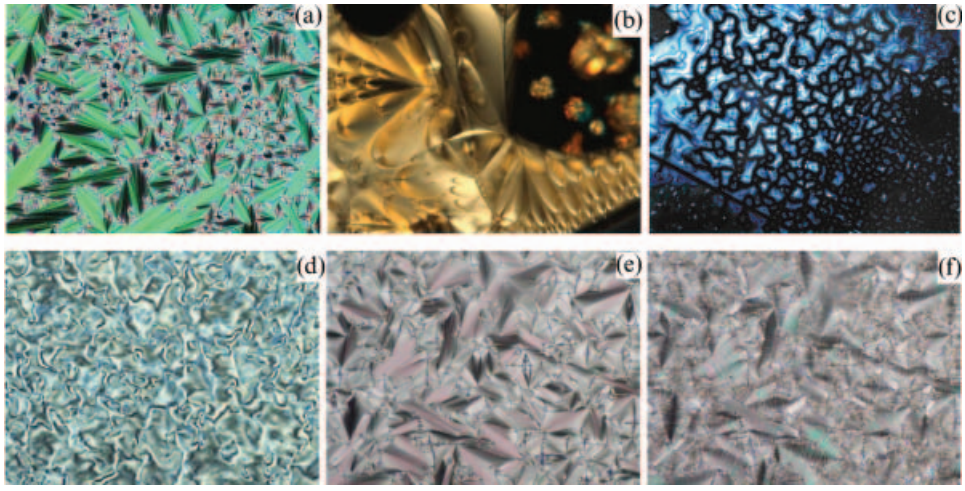

Figure 3. POM images (magnification × 200) showing (a) smectic A mesophase with fan-shaped texture for **1c** at 198°C in the cooling cycle; (b) smectic A mesophase with polygonal texture for **1e** at 289°C in the heating cycle; (c) nematic mesophase with thread-like texture for **1f** at 178°C in the cooling cycle; (d) smectic C mesophase with Schlieren texture for **1f** at 130°C in the cooling cycle; (e) smectic A mesophase with fan-shaped and focal conic textures for **2a** at 110°C in the cooling cycle; (f) soft-crystal E (CrE) phase with striated fan-shaped texture for **2a** at 98°C in the cooling cycle.

three consecutive low-angle diffraction peaks arranged in a periodic order that could be tentatively assigned as [100], [200] and [300] reflections, indicative of the formation of lamellar arrangement of molecules with *d*-spacing values (Å) (26.07 **1a**, 25.86 **1c**, 17.70 **1e**, 27.00 and 23.55 **1f**, 37.49 **2c**; 30.13 **3a**,

Table 3. Phase transition temperatures (T/°C) and enthalpies (ΔH/kJ mol^{-1}) of **1a**–**1f**, **2a**–**2f**, **3a**, **3b**, **4a** and **4b** on the first heating and cooling runs[a].

Compound	Phase transitions[b] T[°C] (ΔH [kJ mol^{-1}])
1a (R=Br)	Cr_1 120.9 (38.10) SmA 244.0 (9.96) Iso
	Iso 241.2 (−8.53) SmA 108.4 (−30.30) Cr_2 95.2 (−3.82) Cr_3
1b (R=Cl)	Cr_1 110.2 (29.37) SmA 236.4 (8.94) Iso
	Iso 233.8 (−9.62) SmA 94.1 (−24.60) Cr_2 67.8 (−3.19) Cr_3
1c (R=F)	Cr_1 88.4 (37.29) SmA 200.8 (7.93) Iso
	Iso 198.4 (−7.66) SmA 71.7 (−33.72) Cr_2
1d (R=CN)	Cr_1 93.7 (9.09) Cr_2 101.6 (14.60) Cr_3 105.6 (8.40) SmA 260.4 (7.76) Iso
	Iso 260.4 (−7.46) SmA 77.9 (−29.43) Cr_4
1e (R=NO_2)	Cr_1 119.1 (35.60) Cr_2 162.8 (11.04) SmA 284.9 (8.38) Iso[c]
1f (R=CH_3)	Cr_1 102.1 (41.88) SmC 136.6 (0.42) N 176.1 (1.27) Iso
	Iso 174.9 (−1.46) N 135.5 (−0.41) SmC 69.5 (−40.62) Cr_2
2a (R=Br)	Cr_1 61.7 (9.01) Cr_2 117.7 (33.51) SmA 120.6 (7.42) Iso
	Iso 118.7 (−7.11) SmA 102.3 (−16.01) CrE 94.9 (−13.91) Cr_3
2b (R=Cl)	Cr_1 57.7 (4.58) Cr_2 97.0 (43.4) SmA 112.0 (12.89) Iso
2c (R=F)	Cr 79.5 (16.28) SmA 86.1 (4.41) Iso
2d (R=CN)	Cr_1 41.3 (3.77) Cr_2 60.8 (3.48) Cr_3 100.1 (2.56) Cr_4 115.6 (2.15) Cr_5 128.1 (20.25) SmA 133.7 (3.35) Iso
	Iso 131.9 (−3.99) SmA 118.6 (−23.97) Cr_6 113.0 (−2.54) Cr_7 82.8 (−0.93) Cr_8 55.3 (−4.38) Cr_9 30.1 (−3.79) Cr_{10}
2e (R=NO_2)	Cr_1 47.5 (7.12) Cr_2 129.7 (20.22) Cr_3 164.7 (22.17) Iso
	Iso 162.0 (−22.72) Cr_4
2f (R=CH_3)	Cr_1 91.4 (14.71) Cr_2 99.7 (35.02) Iso
	Iso 84.4 (−24.24) Cr_3 75.6 (−10.62) Cr_4
3a (R=Cl)	Cr_1 120.8 (41.85) SmA 369.1 Iso[c]
3b (R=F)	Cr_1 94.0 (15.68) Cr_2 117.7 (24.32) SmA 331.5 (7.82) Iso
	Iso 329.9 (−11.02) SmA 83.0 (−25.29) Cr_3
4a (R=Cl)	Cr_1 111.4 26.56) CrE 132.7 (19.63) SmA 215.8 (6.83) Iso
	Iso 214.9 (−6.54) SmA 130.0 (−11.51) CrE 76.3 (−19.37) Cr_2
4b (R=F)	Cr_1 95.4 (18.0) CrE 120.0 (16.9) SmA 180.8 (5.04) Iso
	Iso 179.6 (−4.42) SmA 115.8 (−9.91) CrE 107.1 (−8.48) Cr_2

[a] Cr_n=crystal phase (*n*th); SmA=smectic A mesophase; SmC=smectic C mesophase; N=nematic mesophase; CrE=soft crystal E phase; Iso=isotropic liquid, [b] determined by DSC, [c] partially decomposition.

31.60 **3b**, 30.08 **4a**, 30.38 **4b**). In particular, the 2θ values of the strongest diffraction peaks in the PXRD pattern of **1e** matched the calculated peak positions of the [001] Miller planes of the X-ray crystal structures (Supporting Information, Figure S1, can be found via the multimedia link on the online article webpage). This finding suggests that lamellar arrangements of molecules as found in their X-ray crystal structures predominately existed in the as-synthesised solid sample of **1e**, while some of the solid samples (**1b**, **2a**–**2b** and **2e**) displayed a single diffraction peak that was caused by the effect of preferred orientation due to platy crystallites existing in their bulk samples. The observed *d*-spacing values (Å) (26.52 **1b**, 29.65 **2a**, 26.77 **2b** and 36.91 **2e**) are also comparable with those of the lamellar-like arrangement of molecules of the aforesaid compounds. However, the PXRD patterns of **1d**, **2d** and **2f** showed random distributions of diffraction peaks in the 2θ range of 2–15°, suggesting that non-lamellar and/or close-packing arrangement of molecules were possible in these cases.

2.6 In-situ *variable-temperature X-ray diffraction*

The structural changes associated with phase transitions of solid samples of **1c**, **1e**, **2a**, **2d**, **3a**, **3b**, **4a** and **4b** had been individually monitored using the in-situ VTXRD technique. Figure 4 depicts the X-ray diffractograms recorded when the solid sample of **1c** was heated at 30–210°C and its smectic A phase was cooled at 180–30°C. For the heating process, the 2θ value of the strongest diffraction peak shifted from 3.40° to 3.08° when the temperature increased from 75°C to 100°C. This peak shift together with an increase in relative intensity of this peak was attributed to the crystal-to-mesophase transition. The structure of the smectic A mesophase of **1c** was stable at 190°C and the *d*-spacing value of 28.67 Å represents a well-ordered lamellar arrangement of molecules in the smectic A mesophase, as evidenced by the sharp and strong peak at 3.06°. Later, the mesophase quickly disappeared and formed an isotropic liquid at 210°C. When the isotropic liquid was cooled from 210°C to 180°C, a smectic A mesophase reappeared with a similar peak at 3.05°. Further cooling of this mesophase to room temperature produced a new crystal polymorph (Cr_2) that displayed two diffraction peaks with 2θ values of 3.40° and 6.82°. Replacing the substituents (Br, Cl and F) as the cases in **1a**–**1c** by the NO_2 substituent uniquely led to the formation of a new crystal polymorph (Cr_2) of **1e** prior to its smectic A mesophase (Supporting Information Figure S2). The 2θ value of the strongest diffraction peak was significantly shifted from 5.01° to 2.81° when the temperature increased from 100°C to 130°C. At 200°C, this new crystal polymorph (Cr_2) converted to the respective smectic A mesophase with a 50% drop in relative intensity of the peak at 2.81°. This observation indicated a reduction of internal orders of the molecules in the smectic A phase. At 260–

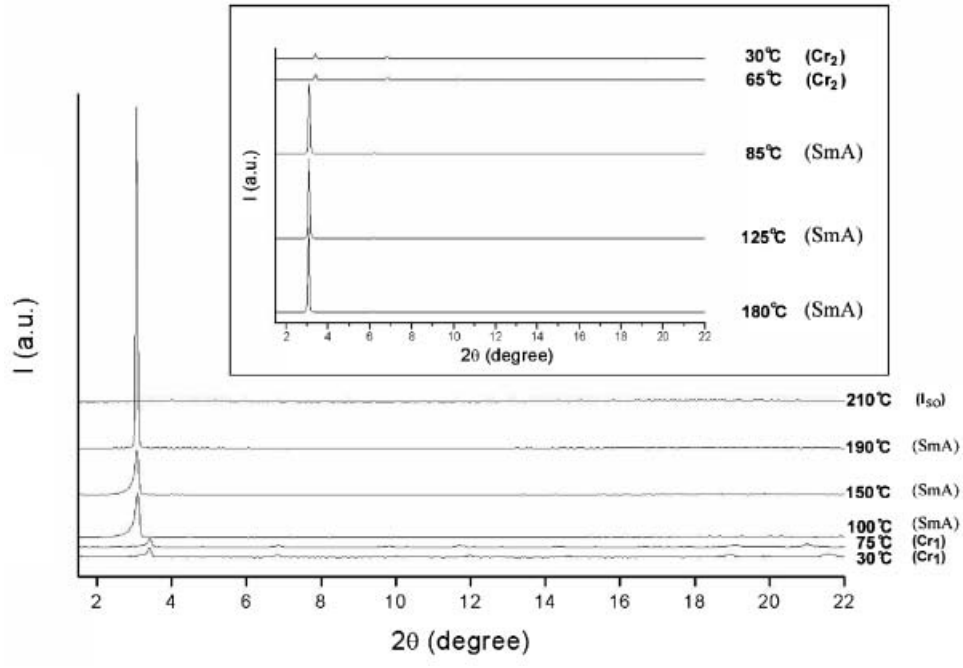

Figure 4. X-ray diffractograms recorded upon heating the solid sample of **1c** and cooling its isotropic liquid (inset).

300°C, the smectic A phase displayed a broad diffraction peak with a *d*-spacing value of 32 Å (2θ=2.7°), which was roughly double of that (17.77 Å) of the original crystalline solid. This implies that a double-layer arrangement of molecules formed. Unfortunately, when the isotropic liquid cooled from 250°C to 30°C, a broad diffraction peak at 2.2° (2θ) was observed, indicating that the solid residue was amorphous and contained a disordered arrangement of molecules.

For **2a**, heating the solid samples from 30°C to 120°C, polymorphic crystal-to-crystal and crystal-to-mesophase transitions occurred at 60°C and 120°C, respectively (Supporting Information Figure S3). For **2d**, several polymorphic crystal-to-crystal transitions occurred at 30–110°C before the smectic A phase appeared at 130°C (Supporting Information Figure S4). The smectic A mesophases of **2a** and **2d** were found to be structurally stable at 120°C and 130°C, respectively.

Figure 5 depicts the X-ray diffractograms recorded upon heating the solid sample of **3a** and cooling its isotropic liquid. The original crystalline solid sample of **3a** displayed the strongest diffraction peak at 2.93° (2θ) and a crystal-to-mesophase transition occurred near 110°C accompanied by an additional weak peak at 2.55° (2θ) with a ratio of their peak areas in 92:8. The relative intensity of this weak peak increased with temperature from 110°C to 250°C, indicative of the formation of smectic A mesophase. Moreover, cooling the isotropic liquid from 250°C to 30°C, the diffractogram of annealed solid residue of **3a** showed a strong diffraction peak at 2.66° and a weak one at 19.5° (2θ). Indeed, compared with the strongest peak of the original crystalline solid of **3a**, the relative intensity of the former peak of the annealed solid residue was apparently larger with a small left-shift in 2θ value by 0.27°. The latter weaker peak of annealed solid residue could be attributed to the appearance of

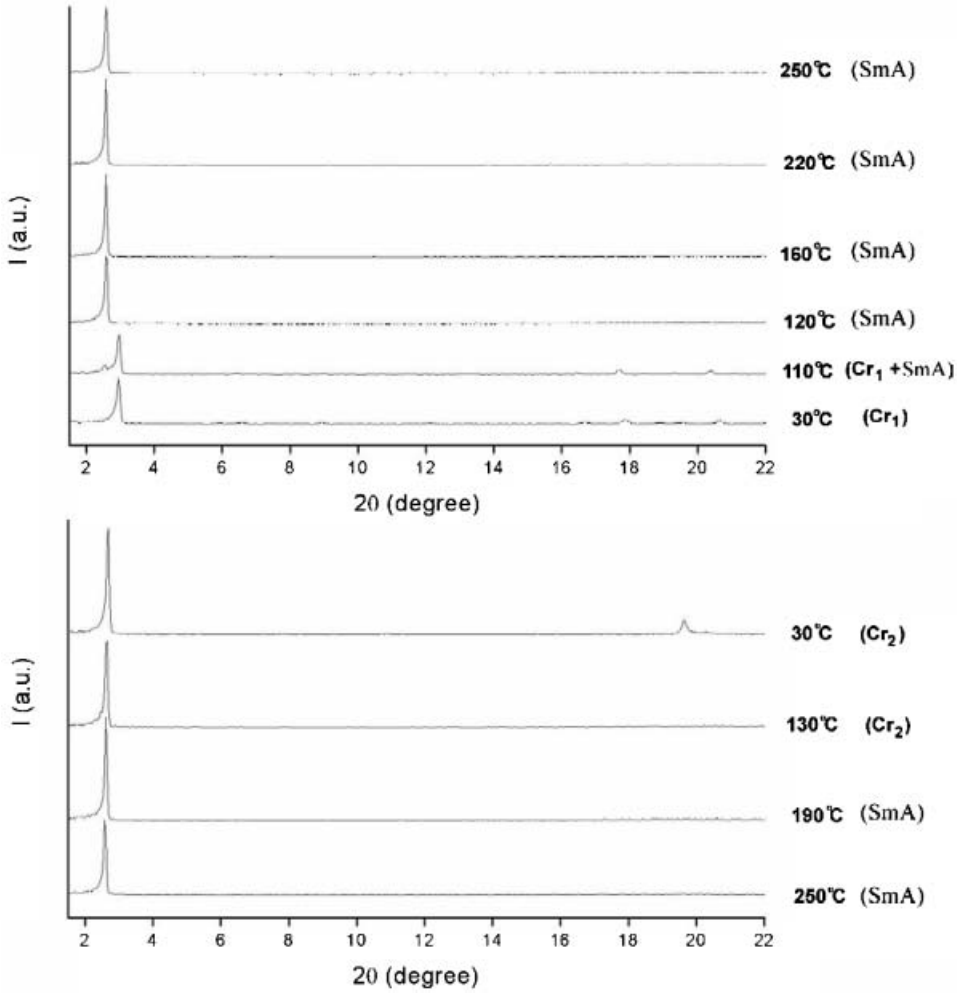

Figure 5. X-ray diffractograms recorded upon heating the solid sample of **3a** (upper) and cooling its isotropic liquid (lower).

lateral short-range orders of *n*-decyl chains of the molecules at a *d*-spacing value of 4.6 Å. As shown by the X-ray diffractograms of **3b** (Supporting Information Figure S5), the crystal-to-crystal and the crystal-to-mesophase transitions for **3b** occurred at 90°C and at around 110–120°C, respectively. Compared with the cases of **3a**–**3b**, the smectic A phase of **4a** and **4b** formed at 130°C and 120°C during the heating process, respectively (Supporting Information Figures S6–7). Later, their smectic A mesophases individually formed isotropic liquid at 220°C and 190°C, respectively. Also, upon heating the original solid samples of **4a** and **4b**, notable peak shifts were found [2.93° (at 90°C)→2.70° (at 120°C) in **4a** and 2.96° (at 80°C)→2.72° (at 90°C) in **4b**]. Such peak shift in 2θ values in both cases were uniquely assigned to the formation of soft crystal E (CrE) phases of **4a** and **4b**.

2.7 *Thermogravimetric analysis*

The thermogravimetric analysis (TGA) curves of solid samples of **1b**, **1c**, **3a**, **3b**, **4a** and **4b** are given in Supporting Information (Figure S8). All solid samples showed no apparent weight loss at 25–250°C, indicative of the absence of occluded solvent of crystallisation. All of them started to lose weight at around 270–320°C in a single step and the whole decomposition process completed near 420–440°C. The decomposition behaviours of the 1,3,4-thiadiazole derivatives **1b**, **1c**, **3a** and **3b** are considerably different from that of 1,3,4-oxadiazole analogues, in which the latter compounds decomposed by a two-step process at 280–700°C (*19*). Inserting one *p*-phenylene spacer unit between the 1,3,4-thiadiazole and the *p*-substituted phenyl (*p*-R-C_6H_4) units of molecules of **1b** and **1c** slightly increased their onset decomposition temperatures from 260–300°C (for **1b** and **1c**) to 300–340°C (for **3a** and **3b**).

3. Discussion

In this study, via slight chemical modifications of these molecular compounds, we found that the extended 1,3,4-thiadiazole derivatives **3a** and **3b** have considerably wide mesomorphic temperature ranges (ΔT or $T_c - T_m$=214–248°C) as seen in Table 1, which represents a rare archetypal example of robust calamitic mesogens. In the literature, Parra and co-workers reported a series of unsymmetric mesogenic 1,3,4-thiadiazole derivatives with short amido, imino and azo linkers (*26, 27, 50*). These compounds usually exhibited narrow or moderate mesomorphic temperature ranges (ΔT=5.2–67.1°C), which are influenced by the length of the terminal alkoxy chains and the central linker moieties. Sato et al. reported quaterphenyl analogues comprising a central bi-1,3,4-thiadiazole unit with wide temperature range of 132.3°C and very high clearing point up to 318.8°C (*51*). In contrast, the comparable mesomorphic temperature ranges of the substituted 2,5-diaryl-1,3,4-thiadiazole and 1,3,4-oxadiazole derivatives in this work are also sensitive to their terminal substituents and the *p*-phenylene spacer, as described below.

3.1 *Effect of heterocyclic ring*

As revealed by the X-ray crystal structure of **1e** and other non-mesogenic 1,3,4-thiadiazole (*45*) and 1,3,4-oxadiazole derivatives (*46*), it is noteworthy to point out that the lone pair of the sulphur (or oxygen) atom of thiadiazole (or oxadiazole) ring involves no intermolecular interactions in the crystalline solids. Thus, for the same type of the terminal substituent, the melting temperatures of each 1,3,4-thiadiazole derivative **1a**–**1e** and the corresponding 1,3,4-oxadiazole analogue **2a**–**2e** are similar to each other, which might be related to structural resemblances in their crystalline solids. The sulphur (or oxygen) atom of the thiadiazole (or oxadiazole) ring plays a role in altering the molecular shape, leading to different liquid crystal behaviours. As observed from the X-ray structure of **1e**, the longer C–*X* bond distances and smaller C–*X*–C angle of the 1,3,4-thiadiazole unit apparently favour the formation of a rod-like molecular geometry with large bent angles (167–169°), which enables more efficient packing of molecules in the respective mesophases, compared with the bent-shaped 1,3,4-oxadiazole analogues (bent angle *ca* 134°). Consequently, the linearity of the molecule generates a larger dipole moment which could readily explain the observation that the 1,3,4-thiadiazole derivatives **1a**–**1f** had higher clearing temperatures and their respective mesophase exhibited wider mesomorphic temperature ranges, compared with that of **2a**–**2f**. The same trends in T_m and T_c also happen for the extended 1,3,4-thiadiazoles (**3a**, **3b**) and 1,3,4-oxadiazoles (**4a**, **4b**). In summary, the substituted 1,3,4-thiadiazole derivatives tend to form more stable mesophases, which might be attributed to their molecular features with large bent angles and large dipole moment perpendicular to the long axis of the molecules. These findings are consistent with those reported previously (*20, 52*). In the literature, the difference in electronegativity between the sulphur and oxygen atoms, which affects the liquid crystal properties, has been discussed (*53*).

3.2 *Effect of terminal substituents*

For a given 1,3,4-thiadiazole or 1,3,4-oxadiazole derivative, changing the terminal substituent of the

molecule readily alters the melting temperatures as a consequence of modifying the molecular packing in the crystalline solids. As shown in Table 1, the melting temperatures of the 1,3,4-thiadiazole and 1,3,4-oxadiazole derivatives decreased in the same orders (Br **1a**>Cl **1b**>F **1c**; Br **2a**>Cl **2b**>F **2c**; Cl **3a**>F **3b**; Cl **4a**>F **4b**). Although the X-ray crystal structures of these halide-containing derivatives have not been obtained, secondary weak interactions such as non-bonded halogen···halogen interactions and non-covalent C–H···*X* hydrogen bonds via the halides atom of the C–*X* bonds (*X*=Br, Cl and F) (*54–60*) are believed to stabilise the packing of molecules in the crystalline solids and their mesophases. The polar and longer C–Br bond of the Br substituent favourably enables a better stabilisation of molecular packing in the crystalline solid. Whilst, in the cases of **1c**, **2c**, **3b** and **4b**, less stable packing of molecules might be formed because the C–F bond is less polar with a very small dipole moment, leading to insignificant intermolecular F···H–C or F···F interactions. Besides, the clearing temperatures similarly followed the same orders as their melting temperatures (**1a**>**1b**>**1c**; **2a**>**2b**>**2c**; **3a**>**3b** and **4a**>**4b**). These observations could be explained by the difference in dipole moments of these compounds. The molecule with a higher polarity generally requires more energy to overcome the lattice stabilisation energy, leading to the occurrence of the mesophase-to-liquid (SmA→Iso) transition at a higher clearing temperature.

The electron-withdrawing C≡N substituent in **1d** plays an important role in stabilisation of the smectic A phase, as revealed by its wide mesomorphic temperature range (ΔT=155°C), compared with that (ΔT=112–126°C) of **1a**–**1c**. The higher T_c value of **1d** is probably caused by an increase in the dipole moment of the molecule, which is attributed to the ability of the polar C≡N group to form an extended π-conjugation with the 1,3,4-thiadiazole and *p*-phenylene rings, as well as the possible C–H···N≡C weak interactions with surrounding aryl/alkyl hydrogen atoms. In the literature, these weak interactions could be regarded as non-covalent hydrogen bonds that appear to adopt either an end-on or a bifurcated geometry (*61–63*). Moreover, the effect of the C≡N substituent on mesomorphic properties of 4-cyano-4-(*n*-octyl)biphenyl and 4-cyano-4-(*n*-octyloxyl)biphenyl had been studied by Fourier transform infrared (FT-IR), Raman spectroscopy and variable-temperature X-ray diffraction, suggesting that there was a decrease in υ(C≡N) stretching frequency together with notable shifts in the 2θ values of diffraction peaks when their respective smectic A mesophases formed (*64, 65*).

Similar to the case in **1d**, the presence of the electron-withdrawing NO_2 group of **1e** broadens the mesomorphic temperature range. As revealed in the X-ray crystal structure of **1e**, extensive weak π···π stacking and non-covalent C–H···O(N) hydrogen bonding interactions definitely enable an efficient packing of molecules in the crystalline solid. The prevalence of all these weak interactions accounts for its high T_m and T_c value, leading to more stabilisation in packing of molecules in the crystalline solid as well as its mesophase. In addition, the π-conjugation formed between the strong electron-withdrawing NO_2 substituent and the attached *p*-phenylene units could generate a larger molecular dipole moment, leading to the formation of a robust smectic A mesophase with a higher clearing temperature of 284°C.

Concurrently, in contrast to the smectic A mesophase of **1a**–**1e**, compound **1f** with an electron-donating methyl substituent tends to form the smectic C and nematic mesophases. The formation of tilted smectic C and nematic phases of **1f** probably originates from the dynamic nature of the freely-rotating methyl substituent which might coherently destroy the positional orders. On the other hand, the free rotation of NO_2 group along the C–N bond of the molecule of **1e** is restricted by the π-conjugation. Compared with **1a**–**1e**, the smaller dipole molecular moment of **1f** leads to lowering of their melting and clearing temperatures. As a result, similar to the cases of **2d** and **2e**, the 1,3,4-oxadiazole analogue **2f** showed no mesomorphic properties under the same condition.

3.3 Effect of p-phenylene spacer

Inserting a *p*-phenylene spacer between the 1,3,4-thiadiazole or 1,3,4-oxadiazole ring and the para-substituted phenyl unit (*p*-*R*-C_6H_4) of the molecules (**1b**, **1c**, **2b**, **2c**) apparently increases their clearing temperatures, rather than their melting temperatures. This change leads to wider mesomorphic temperature ranges for the extended compounds (ΔT/°C=249 **3a**, 214 **3b**, 104 **4a**, 85 **4b**). Notably, the increase in the length-to-width ratio of each extended molecule generates a larger dipole moment and also enhances the mesogenic character of the molecule, leading to the formation of a smectic A mesophase with higher T_c. In the literature, a recent study on liquid crystal properties of a class of paracyclophane-based mesogen containing a 2,5-diphenyl-1,3,4-thiadiazole unit and two polyether chains connected by a *p*-phenylene, *p*-biphenylene or *p*-terphenylene spacer unit suggested that increasing the mesogenic core length of the paracycloplane macrocycle from *p*-phenylene to *p*-terphenylene spacer unit similarly led to wide

mesomorphic temperature range (ΔT) up to 280°C (*66*).

4. Conclusions

In summary, a series of new liquid crystalline materials derived from substituted 2,5-diaryl-1,3,4-thiadiazole derivatives were prepared by using a microwave-assisted and solvent-free synthetic approach. The crystal structure of **1e** and packing of molecules in crystalline solids have been determined by single-crystal X-ray diffraction. The mesomorphic properties of all these compounds have been compared with the corresponding 1,3,4-oxadiazole analogues. Regarding the relatively narrower mesomorphic temperature ranges of liquid crystals derived from 1,3,4-oxadiazole-containing compounds, we envisioned that simply changing the heteroatom type of the [XC_2N_2] ring moiety of this class from X=O (in 1,3,4-oxadiazole) to S (in 1,3,4-thiadiazole) could significantly broaden the mesomorphic temperature range by at least 100°C in the difference between their melting T_m and clearing T_c temperatures, leading to the formation of robust mesogenic materials. Notably, the extended substituted 2,5-diaryl-1,3,4-thiadiazole derivatives (**3a**–**3b**) demonstrated the widest mesomorphic temperature ranges of ΔT=214–248°C among the compounds in this work. By modifying the terminal substituents and the number of *p*-phenylene spacers, the liquid crystalline properties of all these 1,3,4-thiadiazole derivatives could be tailored by forming nematic N, smectic C or smectic A mesophase, in the absence of soft crystal E phase as found in 1,3,4-oxadiazole analogues.

5. Experimental Section

5.1 General

All starting materials were commercially available and used as received. Dichloromethane used for photoluminescence studies was of high performance liquid chromatography grade, other solvents used were of analytical grade. N-(4-decanoxybenzoyl)hydrazide and the reaction intermediates of **Ic** and **2c** were prepared by the previous methods (*19*). FT-IR spectra of solid sample in KBr pellet form were recorded on Bio-Rad FTS 6000 spectrometer. UV-visible electronic absorption spectra were recorded with a Perkin-Elmer Lambda 19 UV/Vis spectrophotometer. ^{1}H nuclear magnetic resonance (NMR) spectra were collected on Bruker AVANCE (300 MHz) or Varian Mercury Plus 400 (400 MHz) spectrometer with chemical shifts (in ppm scale) relative to tetramethylsilane (δ=0 ppm). Proton decoupled ^{13}C NMR spectra were recorded at 101 MHz on the same NMR spectrometer. Elemental analyses were performed on a YANACO CHN CORDER MT-3 apparatus. Electrospray ionisation mass spectra (ESI-MS) were recorded on Finnigan LCQ Advantage spectrometer and high-resolution mass spectra (HRMS) using the electron impact (EI) method were collected with the Finnigan MAT 95 mass spectrometer. Intensity data of single crystals of **1e** were collected using a Rigaku diffractometer with graphite-monochromatized MoK_α X-ray radiation (λ=0.71073 Å) and Saturn CCD area detector. The X-ray data were collected at −160°C and a maximum 2θ value of 55.8° was attained. A total of 405 oscillation images were collected at three different ϕ angles (0°, 90° and 180°). The ω scans from −110.0° to 70.0° (40° and −35° for ϕ=90° and 180° respectively) in 1.0° step increment, at χ=45.0° was used with an exposure rate of 1.0° per second. The detector swing angle was −19.89° and the crystal-to-detector distance was 45.03 mm. The X-ray crystal structure of **1e** was solved by the direct method and expanded using Fourier syntheses technique. All the non-hydrogen atoms in this structure were refined anisotropically. The positions of the hydrogen atoms were calculated from idealised geometry of the attached parent atoms and the positions and thermal parameters were refined using a riding model. Structural refinement based on the full-matrix least-squares refinement on $|F|^2$ values was performed by using CrystalStructure or SHELXL97 suite program (*67–69*).

Step-scanned PXRD data of solid samples were collected at room temperature on a Bruker D8 ADVANCE diffractometer with CuK_α X-ray radiation (λ=1.54183 Å, rated at 1.6 kW). The *in situ* variable-temperature X-ray diffractograms were recorded using the same diffractometer equipped with a modular temperature chamber attachment (Material Research Instruments) operating at 30–300°C. Scan range=1.5–22° (2θ), step size=0.04° (2θ), scan time=1s per step were used. The rate of temperature change was 0.5°C per second.

Steady-state emission spectra were recorded with SPEX 1681 Fluorolog-2 series F111AI spectrophotometer. Solution samples for measurements were degassed with three freeze-pump-thaw cycles. The phase transition temperatures and enthalpy changes were measured on NETZSCH DSC 204 differential scanning calorimeter at a heating rate of 5°C/min and calibrated with a pure indium sample. The POM texture image of mesophase was recorded using a polarised-light optical microscope (OLYMPUS BX51) equipped with a

temperature-controlled hot stage. Thermogravimetric analyses of solid samples of **1b**, **1c**, **3a**, **3b**, **4a** and **4b** were performed by Perkin-Elmer TGA-7 under a stream of flowing N_2.

5.2 Synthesis and characterisation

5.2.1 Preparation of Ia–If.

The preparation of the intermediate **Ia**–**If** was slightly modified, according to our previously method (*19*). To a round-bottom flask (100 ml) were added *p*-substituted benzoic acid *R*-$PhCO_2H$ (10 mmol, 1.4–2.8 g) (*R*=Br, Cl, F, CN, NO_2, CH_3) and thionyl chloride $SOCl_2$ (10 ml). The mixture was refluxed for 5 h to give the corresponding *p*-substituted benzoyl chloride. Excessive $SOCl_2$ was removed by vacuum distillation and *p*-decyloxybenzoic hydrazide (10 mmol, 2.92 g) dissolved in pyridine (15 ml) was added dropwise to the as-formed *p*-substituted benzoyl chloride. The reaction mixture was stirred at room temperature for 2 h and then at 70°C for further 1 h. Crude solid was precipitated by pouring the reaction mixture into distilled water (50 ml). The crude solid was washed with distilled water and recrystallised from ethanol. Yield: 70–80%.

4-Bromobenzoic acid N′-(4-decyloxybenzoyl)hydrazide **Ia**: ^{1}H-NMR ($CDCl_3$): δ (ppm)=9.29 (s, 1H), 9.08 (s, 1H), 7.82 (d, *J*=8.7 Hz, 2H), 7.74 (d, *J*=8.7 Hz, 2H), 7.62 (d, *J*=8.7 Hz, 2H), 6.96 (d, *J*=8.7 Hz, 2H), 4.02 (t, *J*=6.6 Hz, 2H), 1.89–1.74 (m, 2H), 1.53–1.16 (m, 14H), 0.89 (t, *J*=6.6 Hz, 3H). ^{13}C-{^{1}H}-NMR (DMSO): δ (ppm)=165.99, 165.70, 162.22, 132.45, 132.24, 130.23, 130.06, 126.30, 125.19, 114.81, 68.43, 32.01, 29.72, 29.68, 29.48, 29.41, 29.30, 26.19, 25.11, 22.81, 14.63. ESI (+ve): 475.37 (M^+, 100). HRMS Calcd for $C_{24}H_{32}BrN_2O_3$: 475.1591; Found: 475.1593. FT-IR (KBr) (cm^{-1}): 3214.8, 2919.4, 2852.7, 1600.6, 1560.4, 1515.9, 1462.4, 1376.9, 1303.1, 1254.9, 1174.7, 1108.2, 1012.6, 841.8, 744.6, 721.7.

4-Chlorobenzoic acid N′-(4-decyloxybenzoyl)hydrazide **Ib**: ^{1}H-NMR ($CDCl_3$): δ (ppm)=9.31 (s, 1H), 9.08 (s, 1H), 7.81 (d, *J*=7.2 Hz, 4H), 7.45(d, *J*=7.2 Hz, 2H), 6.95 (d, *J*=7.2 Hz, 2H), 4.01 (t, *J*=6.6 Hz, 2H), 1.89–1.73 (m, 2H), 1.49–1.20 (m, 14H), 0.89 (t, *J*=6.6 Hz, 3H). ^{13}C-{^{1}H}-NMR ($CDCl_3$): δ (ppm)=165.24, 164.79, 161.44, 136.62, 131.29, 129.26, 128.47, 124.37, 113.97, 67.63, 31.22, 28.93, 28.88, 28.69, 28.62, 28.51, 25.40, 22.02, 13.85. MS (20 eV, EI) *m*/*z* (*I* %): 430 (2.07) $[M]^+$. HRMS Calcd for $C_{24}H_{31}ClN_2O_3$: 430.2023; Found: 430.2023. FT-IR (KBr) (cm^{-1}): 3223.7, 2922.8, 2852.8, 1599.3, 1563.5, 1518.0, 1494.4, 1466.7, 1377.0, 1304.3, 1260.6, 1177.8, 1097.9, 1016.9, 842.5, 810.3, 747.0, 722.4.

4-Fluorobenzoic acid N′-(4-decyloxybenzoyl)hydrazide **Ic**: ^{1}H-NMR ($CDCl_3$): δ (ppm)=9.50 (d, *J*=6.6 Hz, 1H), 9.22 (d, *J*=6.6 Hz, 1H), 7.88 (q, *J*=8.4 Hz, 2H), 7.82 (d, *J*=8.8 Hz, 2H), 7.12 (d, *J*=8.4 Hz, 2H), 6.92 (d, *J*=8.8 Hz, 2H), 4.00 (t, *J*=6.6 Hz, 2H), 1.81 (m, 2H), 1.46 (m, 2H), 1.30 (m, 12H), 0.88 (t, *J*=6.6 Hz, 3H). ^{13}C-{^{1}H}-NMR ($CDCl_3$): δ (ppm)=165.31, 164.82, 162.46, 161.43, 130.01, 129.06, 129.02, 124.39, 115.56, 114.06, 67.65, 31.21, 28.91, 28.86, 28.66, 28.60, 28.48, 25.38, 22.00, 13.85. MS (20 eV, EI) *m*/*z* (*I* %): 414 (3.31) $[M]^+$. HRMS Calcd for $C_{24}H_{31}FN_2O_3$: 414.2318; Found: 414.2318. FT-IR (KBr): 3218.2, 2923.4, 2852.8, 1605.6, 1588.3, 1574.0, 1517.8, 1469.9, 1454.9, 1377.7, 1305.6, 1262.0, 1174.4, 1117.9, 1098.0, 1019.5, 844.2, 750.3, 721.4.

4-Cyanobenzoic acid N′-(4-decyloxybenzoyl)hydrazide **Id**: ^{1}H-NMR ($CDCl_3$): δ (ppm)=10.14 (s, 1H), 9.34 (s, 1H), 7.96 (d, *J*=7.8 Hz, 2H), 7.79 (d, *J*=8.4 Hz, 2H), 7.64 (d, *J*=7.8 Hz, 2H), 7.00 (d, *J*=8.4 Hz, 2H), 4.00 (t, *J*=6.6 Hz, 2H), 1.88–1.74 (m, 2H), 1.57–1.20 (m, 14H), 0.88 (t, *J*=6.6 Hz, 3H). ^{13}C-{^{1}H}-NMR (DMSO): δ (ppm)=165.22, 162.25, 137.22, 133.32, 130.05, 128.93, 124.93, 118.88, 114.84, 68.41, 31.97, 29.67, 29.62, 29.42, 29.36, 29.24, 26.14, 22.77, 14.62. ESI (–ve): 420.32 (M^+). HRMS Calcd for $C_{25}H_{32}N_3O_3$: 422.2438; Found: 422.2438. FT-IR (KBr) (cm^{-1}): 3198.3, 2924.1, 2852.3, 2228.8, 1597.0, 1576.0, 1558.3, 1513.5, 1501.5, 1466.0, 1377.1, 1303.9, 1256.5, 1170.6, 1111.0, 1017.4, 840.5, 813.7, 751.6, 721.1.

4-Nitrobenzoic acid N′-(4-decyloxybenzoyl) hydrazide **Ie**: ^{1}H-NMR ($CDCl_3$): δ (ppm)=9.67 (s, 1H), 9.13 (s, 1H), 8.32 (d, *J*=8.7 Hz, 2H), 8.06 (d, *J*=8.7 Hz, 2H), 7.82 (d, *J*=8.7 Hz, 2H), 6.96 (d, *J*=8.7 Hz, 2H), 4.02 (t, *J*=6.6 Hz, 2H), 1.86–1.77 (m, 2H), 1.52–1.21 (m, 14H), 0.89 (t, *J*=6.6 Hz, 3H). ^{13}C-{^{1}H}-NMR (DMSO): δ (ppm)=165.92, 165.04, 162.27, 150.08, 138.87, 130.07, 129.65, 124.90, 124.43, 114.85, 68.41, 31.97, 29.68, 29.63, 29.43, 29.37, 29.24, 26.14, 22.77, 14.62, ESI (–ve): 440.27 (M^+). HRMS Calcd for $C_{24}H_{32}N_3O_5$: 442.2337; Found: 442.2340. FT-IR (KBr) (cm^{-1}): 3197.8, 2924.6, 2853.0, 1608.3, 1590.6, 1566.6, 1522.7, 1494.7, 1465.6, 1376.9, 1345.2, 1256.5, 1174.4, 1109.6, 1028.2, 844.8, 809.4, 758.2, 721.5.

4-Methylbenzoic acid N′-(4-decyloxybenzoyl)hydrazide **If**: ^{1}H-NMR ($CDCl_3$): δ (ppm)=10.30 (s, 2H), 7.83 (d, *J*=7.8 Hz, 2H), 7.76 (d, *J*=8.1 Hz, 2H), 7.25 (d, *J*=7.8 Hz, 2H), 6.92 (d, *J*=8.2 Hz, 2H), 4.00 (t, *J*=6.5 Hz, 2H), 2.41 (s, 3H), 1.75–1.84 (m, 2H), 1.28–1.49 (m, 14H), 0.88 (t, *J*=6.6 Hz, 3H). ^{13}C-{^{1}H}-NMR (DMSO-d_6): δ (ppm)=14.56, 21.63, 22.70, 26.07, 29.18, 29.29, 29.35, 29.55, 29.60, 31.90, 68.34,

114.75, 118.32, 125.22, 128.07, 129.61, 129.94, 142.37, 162.08, 165.96, 166.02. MS (20 eV, EI) *m/z* (*I* %): 411 (4.18) [M$^+$]. HRMS Calcd for $C_{25}H_{34}N_2O_3$: 410.2569; Found: 410.2569.

5.2.2 *Synthesis of **1a–1f**.*

The intermediate compounds **Ia**–**If** (1 mmol) and Lawesson's reagent [2,4-bis-(4-methoxyphenyl)-1,3-dithia-2,4-diphosphetane-2,4-disulphide] (1.1 mmol) were mixed and placed into a test tube (10 ml), which was placed into a household microwave oven (Glanz WP800TL23-KL) and radiated at a full power (800 W). When the mixture turned into a brown liquid, the microwave irradiation was stopped immediately. The crude product was purified by silica gel column chromatography using ethyl acetate/dichloromethane mixture (v/v=1:15) as an eluent. Yields: 45–75%.

2-(4-Bromophenyl)-5-(4-decyloxyphenyl)-1,3,4-thiadiazole **1a**: ^{1}H-NMR ($CDCl_3$): δ (ppm)=7.95 (d, *J*=8.7 Hz, 2H), 7.87 (d, *J*=8.7 Hz, 2H), 6.63 (d, *J*=8.7 Hz, 4H), 6.99 (d, *J*=8.7 Hz, 2H), 4.03 (t, *J*=6.6 Hz, 2H), 1.86–1.77 (m, 2H), 1.54–1.72 (m, 14H), 0.89 (t, *J*=6.6 Hz, 3H). ^{13}C-{^{1}H}-NMR ($CDCl_3$): δ (ppm)=168.41, 166.17, 161.83, 132.50, 129.63, 129.41, 129.28, 125.41, 122.53, 115.22, 68.45, 32.03, 29.70, 29.51, 29.45, 29.28, 26.14, 22.82, 14.25. MS (20 eV EI) *m/z* (*I* %): 473 (6.53) [M]$^+$. HRMS Calcd for $C_{24}H_{29}BrN_2OS$: 472.1184; Found: 472.1184. Elemental analyses (%): calculated for C: 60.88, H: 6.17, N: 5.92; found C: 60.45, H: 6.37, N: 5.73. FT-IR (KBr) (cm^{-1}): 2920.7, 2852.9, 1601.9, 1516.0, 1492.0, 1467.0, 1444.5, 1407.7, 1301.8, 1261.3, 1179.8, 1090.1, 1072.0, 1024.1, 986.7, 824.1, 601.2.

2-(4-Chlorophenyl)-5-(4-decyloxyphenyl)-1,3,4-thiadiazole **1b**: ^{1}H-NMR ($CDCl_3$): δ (ppm)=7.94 (d, *J*=7.8 Hz, 4H), 7.47 (d, *J*=8.4 Hz, 2H), 6.99 (d, *J*=8.4 Hz, 2H), 4.03 (t, *J*=6.6 Hz, 2H), 1.86–1.77 (m, 2H), 1.55–1.18 (m, 14H), 0.89 (t, *J*=6.6 Hz, 3H). ^{13}C-{^{1}H}-NMR ($CDCl_3$): δ (ppm)=168.41, 166.12, 162.49, 161.84, 137.11, 129.65, 129.57, 129.13, 122.57, 115.24, 68.47, 32.05, 29.71, 29.53, 29.47, 29.29, 26.15, 22.84, 14.27. MS (20 eV EI) *m/z* (*I* %): 429 (34.39) [M]$^+$. HRMS Calcd for $C_{24}H_{29}ClN_2OS$: 428.1689; Found: 428.1689. Elemental analyses (%): calculated for C: 67.19, H: 6.81, N: 6.53; found C: 66.89, H: 6.52, N: 6.35. FT-IR (KBr) (cm^{-1}): 2920.4, 2853.0, 1601.9, 1516.8, 1496.9, 1466.8, 1445.1, 1407.6, 1396.2, 1301.6, 1261.1, 1179.9, 1092.7, 1018.3, 987.2, 828.3, 721.9.

2-(4-Fluorophenyl)-5-(4-decyloxyphenyl)-1,3,4-thiadiazole **1c**: ^{1}H-NMR ($CDCl_3$): δ (ppm)=8.02–7.98 (m, 2H), 7.95 (d, *J*=8.4 Hz, 2H), 7.19 (t, *J*=8.4 Hz, 2H), 7.00 (d, *J*=8.7 Hz, 2H), 4.03 (t, *J*=6.6 Hz, 2H), 1.86–1.77 (m, 2H), 1.56–1.08 (m, 14H), 0.89 (t, *J*=6.6 Hz, 3H). ^{13}C-{^{1}H}-NMR ($CDCl_3$): δ (ppm)=168.19, 166.10, 162.63 (d, J_{C-F}=8.1 Hz), 161.78, 129.94 (d, J_{C-F}=3.4 Hz), 129.60, 126.85, 122.64, 116.47 (d, J_{C-F}=8.8 Hz), 115.22, 68.46, 32.05, 29.72, 29.53, 29.47, 29.30, 26.16, 22.84, 14.27. MS (20 eV EI) *m/z* (*I* %): 413 (28.49) [M]$^+$. HRMS Calcd for $C_{24}H_{29}FN_2OS$: 412.1985; Found: 412.1985. Elemental analyses (%): calculated for C: 69.87, H: 7.09, N: 6.79; found C: 69.72, H: 7.00, N: 6.79. FT-IR (KBr) (cm^{-1}): 2920.2, 2851.2, 1607.5, 1516.8, 1462.7, 1454.6, 1377.5, 1314.1, 1241.8, 1178.0, 1086.4, 1023.7, 988.0, 837.6, 816.4, 723.7.

2-(4-Cyanophenyl)-5-(4-decyloxyphenyl)-1,3,4-thiadiazole **1d**: ^{1}H-NMR ($CDCl_3$): δ (ppm)=8.13 (d, *J*=8.4 Hz, 2H), 7.94 (d, *J*=8.7 Hz, 2H), 7.79 (d, *J*=8.4 Hz, 2H), 7.00 (d, *J*=8.7 Hz, 2H), 4.03 (t, *J*=6.6 Hz, 2H), 1.88–1.77 (m, 2H), 1.56–1.14 (m, 14H), 0.89 (t, *J*=6.6 Hz, 3H). ^{13}C-{^{1}H}-NMR ($CDCl_3$): δ (ppm)=169.40, 165.11, 162.13, 134.44, 133.02, 129.79, 128.32, 122.18, 118.25, 115.31, 114.31, 68.50, 32.03, 29.69, 29.50, 29.45, 29.26, 26.13, 22.81, 14.25. MS (20 eV EI) *m/z* (*I* %): 420 (6.14) [M]$^+$. HRMS Calcd for $C_{25}H_{29}N_3OS$: 419.2031; Found: 419.2031. Elemental analyses (%): calculated for C: 71.56, H: 6.97, N: 10.01; found C: 70.72, H: 6.70, N: 9.84. FT-IR (KBr) (cm^{-1}): 2921.3, 2853.2, 2223.9, 1601.7, 1518.3, 1462.8, 1407.5, 1377.2, 1302.1, 1262.2, 1172.7, 1092.6, 1013.4, 987.9, 842.4, 828.5, 721.7.

2-(4-Nitrophenyl)-5-(4-decyloxyphenyl)-1,3,4-thiadiazole **1e**: ^{1}H-NMR ($CDCl_3$): δ (ppm)=8.36 (d, *J*=8.7 Hz, 2H), 8.19 (d, *J*=8.7 Hz, 2H), 7.97 (d, *J*=8.7 Hz, 2H), 7.01 (d, *J*=8.7 Hz, 2H), 4.04 (t, *J*=6.6 Hz, 2H), 1.87–1.78 (m, 2H), 1.58–1.15 (m, 14H), 0.89 (t, *J*=6.6 Hz, 3H). ^{13}C-{^{1}H}-NMR ($CDCl_3$): δ (ppm)=169.73, 164.69, 162.23, 149.11, 136.17, 129.87, 128.66, 124.60, 122.17, 115.38, 68.54, 32.05, 29.71, 29.52, 29.47, 29.27, 26.15, 22.83, 14.26. MS (20 eV EI) *m/z* (*I* %): 440 (31.55) [M]$^+$. HRMS Calcd for $C_{24}H_{29}N_3O_3S$: 439.1929; Found: 439.1930. Elemental analyses (%): calculated for C: 65.58, H: 6.65, N: 9.56; found C: 65.30, H: 7.18, N: 9.61. FT-IR (KBr) (cm^{-1}): 2923.8, 2853.1, 1601.9, 1543.3, 1519.4, 1498.9, 1338.5, 1311.6, 1263.6, 1173.3, 1095.6, 1015.7, 989.0, 857.9, 827.6, 721.0.

2-(4-Methylphenyl)-5-(4-decyloxyphenyl)-1,3,4-thiadiazole **1f**: ^{1}H-NMR ($CDCl_3$): δ (ppm)=0.88 (t, *J*=6.6 Hz, 3H), 1.28–1.49 (m, 14H), 1.76–1.85 (m, 2H), 2.42 (s, 3H), 4.01 (t, *J*=6.6 Hz, 2H), 6.97 (d, *J*=8.8 Hz, 2H), 7.28 (d, *J*=8.1 Hz, 2H), 7.88 (d, *J*=8.1 Hz, 2H), 7.92 (d, *J*=8.8 Hz, 2H); ^{13}C-{^{1}H}-NMR ($CDCl_3$): 14.22, 21.59, 22.79, 26.11, 29.27, 29.43, 29.50, 29.68, 32.01, 68.38, 115.12, 122.82,

127.75, 127.85, 129.49, 129.90, 141.39, 161.58, 167.46, 167.67. MS(EI): *m/z*: 409 (39.62) $[M]^+$. HRMS Calcd for $C_{25}H_{32}N_2OS$: 408.2235; Found: 408.2235. Elemental analyses (%): calculated for $C_{25}H_{32}N_2OS$ (%): C 73.49, H 7.89, N 6.86; found C 73.65, H 8.08, N 6.70. FT-IR (KBr) (cm^{-1}): 2921, 2849, 1605, 1519, 1444, 1406, 1266, 1175, 833, 819, 726.

5.2.3 *Synthesis of **2a**–**2f**.*

The intermediate compound **Ia**–**If** (1 mmol) was added to $SOCl_2$ (5 ml) in dried benzene (10 ml). The reaction mixture was refluxed for 7 h and the excessive thionyl chloride and solvent were removed by vacuum distillation. The crude solid was collected and washed several times with distilled water and was further purified by silica gel column chromatography using ethyl acetate/petroleum ether (v/v=1:3) as an eluent. The reaction products were obtained as off-white solids in 75–85% yield.

2-(4-Bromophenyl)-5-(4-decyloxyphenyl)-1,3,4-oxadiazole **2a**: ^{1}H-NMR ($CDCl_3$): δ (ppm)=8.04 (d, *J*=8.7 Hz, 2H), 7.98 (d, *J*=8.4 Hz, 2H), 7.66 (d, *J*=8.4 Hz, 2H), 7.01 (d, *J*=8.7 Hz, 2H), 4.03 (t, *J*=6.6 Hz, 2H), 1.86–1.77 (m, 2H), 1.55–1.20 (m, 14H), 0.89 (t, *J*=6.6 Hz, 3H). ^{13}C-{^{1}H}-NMR ($CDCl_3$): δ (ppm)=164.92, 163.50, 162.26, 132.52, 128.86, 128.34, 126.28, 123.19, 116.06, 115.17, 68.47, 32.05, 29.71, 29.53, 29.48, 29.28, 26.16, 22.84, 14.27. MS (20 eV EI) *m/z* (*I* %): 457 (48.35) $[M]^+$. HRMS Calcd for $C_{24}H_{29}BrN_2O_2$: 456.1412; Found: 456.1412. Elemental analyses (%): calculated for C: 63.02, H: 6.39, N: 6.12; found C: 63.05, H: 6.41, N: 6.12. FT-IR (KBr) (cm^{-1}): 2920.5, 2849.0, 1612.4, 1586.6, 1496.6, 1465.6, 1403.8, 1384.1, 1305.8, 1251.1, 1175.7, 1102.1, 1075.5, 1007.9, 839.0, 810.1, 741.4, 530.3.

2-(4-Chlorophenyl)-5-(4-decyloxyphenyl)-1,3,4-oxadiazole **2b**: ^{1}H-NMR ($CDCl_3$): δ (ppm)=8.09–8.04 (m, 4H), 7.51 (d, *J*=8.7 Hz, 2H), 7.02 (d, *J*=8.7 Hz, 2H), 4.04 (t, *J*=6.6 Hz, 2H), 1.87–1.78 (m, 2H), 1.51–1.48 (m, 14H), 0.887 (t, *J*=6.6 Hz, 3H). ^{13}C-{^{1}H}-NMR ($CDCl_3$): δ (ppm)=164.93, 163.44, 162.26, 137.89, 129.57, 128.87, 128.22, 122.78, 116.10, 115.18, 68.48, 32.04, 29.70, 29.52, 29.46, 29.28, 26.15, 22.82, 14.250. MS (20 eV EI) *m/z* (*I* %): 412 (46.31) $[M]^+$. HRMS Calcd for $C_{24}H_{29}ClN_2O_2$: 412.1917; Found: 412.1917. Elemental analyses (%): calculated for C: 69.80, H: 7.08, N: 6.78; found C: 69.21, H: 7.33, N: 6.76.

2-(4-Fluorophenyl)-5-(4-decyloxyphenyl)-1,3,4-oxadiazole **2c**: ^{1}H-NMR ($CDCl_3$): δ (ppm)=8.12 (m, 2H), 8.04 (d, *J*=8.6 Hz, 2H), 7.22 (m, 2H), 7.01 (d, *J*=8.6 Hz, 2H), 4.03 (t, *J*=6.6 Hz, 2H), 1.82 (m, 2H), 1.48 (m, 2H), 1.30 (m, 12H), 0.88 (t, *J*=6.6 Hz, 3H). ^{13}C-{^{1}H}-NMR ($CDCl_3$): δ (ppm)=166.50, 163.47, 163.15, 162.19, 129.16, 128.82, 120.61, 116.66, 116.37, 115.17, 68.46, 32.03, 29.70, 29.51, 29.45, 29.27, 26.14, 22.82, 14.25. MS (70 eV EI) *m/z* (*I* %): 396 (44.77) $[M]^+$. HRMS Calcd for $C_{24}H_{29}FN_2O_2$: 396.2213; Found: 396.2213. Elemental analyses (%): calculated for C: 72.75, H 7.37, N 7.07. Found: C 72.62, H 7.09, N 7.14.

2-(4-Cyanophenyl)-5-(4-decyloxyphenyl)-1,3,4-oxadiazole **2d**: ^{1}H-NMR ($CDCl_3$): δ (ppm)=8.25 (d, *J*=8.4 Hz, 2H), 8.07 (d, *J*=8.7 Hz, 2H), 7.833 (d, *J*=8.4 Hz, 2H), 7.03 (d, *J*=8.7 Hz, 2H), 4.05 (t, *J*=6.6 Hz, 2H), 1.85–1.74 (m, 2H), 1.56–1.08 (m, 14H), 0.89 (t, *J*=6.6 Hz, 3H). ^{13}C-{^{1}H}-NMR ($CDCl_3$): δ (ppm)=165.55, 162.68, 162.54, 132.98, 129.03, 128.66, 128.13, 127.33, 118.10, 115.64, 115.27, 68.51, 32.02, 29.68, 29.49, 29.44, 29.24, 26.12, 22.81, 14.24. MS (20 eV EI) *m/z* (*I* %): 404 (30.30) $[M]^+$. HRMS Calcd for $C_{25}H_{29}N_3O_2$: 403.2259; Found: 403.2260. Elemental analysis (%): calculated for C: 74.41, H: 7.24, N: 10.41; found C: 74.19, H: 6.94, N: 10.24. FT-IR (KBr) (cm^{-1}): 2920.2, 2849.2, 2231.8, 1610.2, 1494.1, 1465.9, 1390.2, 1302.1, 1257.4, 1176.1, 1102.9, 1023.6, 849.8, 836.8, 744.1.

2-(4-Nitrophenyl)-5-(4-decyloxyphenyl)-1,3,4-oxadiazole **2e**: ^{1}H-NMR ($CDCl_3$): δ (ppm)=8.36 (d, *J*=8.7 Hz, 2H), 8.19 (d, *J*=8.7 Hz, 2H), 7.97 (d, *J*=8.7 Hz, 2H), 7.01 (d, *J*=8.7 Hz, 2H), 4.04 (t, *J*=6.6 Hz, 2H), 1.87–1.78 (m, 2H), 1.58–1.15 (m, 14H), 0.89 (t, *J*=6.6 Hz, 3H). ^{13}C-{^{1}H}-NMR ($CDCl_3$): δ (ppm)=165.76, 162.62, 162.50, 149.54, 129.76, 129.10, 127.76, 124.53, 115.56, 115.30, 68.53, 32.02, 29.69, 29.49, 29.44, 29.24, 26.12, 22.81, 14.24. MS (20 eV EI) *m/z* (*I* %): 424 (25.81) $[M]^+$. HRMS Calcd for $C_{24}H_{29}N_3O_4$: 423.2158; Found: 423.2158. Elemental analyses (%): calculated for C: 68.06, H: 6.90, N: 9.92; found C: 68.17, H: 6.65, N: 10.02. FT-IR (KBr) (cm^{-1}): 2920.1, 2849.9, 1611.5, 1555.4, 1540.0, 1495.8, 1466.0, 1349.4, 1309.2, 1251.1, 1176.1, 1102.1, 1070.0, 854.4, 841.4, 738.4.

2-(4-Methylphenyl)-5-(4-decyloxyphenyl)-1,3,4-oxadiazole **2f**: ^{1}H-NMR ($CDCl_3$): δ (ppm)=0.89 (t, *J*=6.8Hz, 3H), 1.28–1.50 (m, 14H), 1.79–1.86 (m, 2H), 2.44 (s, 3H), 4.04 (t, *J*=6.6Hz, 2H), 7.02 (d, *J*=8.8Hz, 2H), 7.33 (d, *J*=8.0Hz, 2H), 8.01 (d, *J*=8.1Hz, 2H), 8.06 (d, *J*=8.8Hz, 2H). ^{13}C-{^{1}H}-NMR ($CDCl_3$): δ (ppm)=14.24, 21.77, 22.81, 26.14, 29.09, 29.28, 29.45, 29.51, 29.69, 32.03, 68.43, 115.11, 116.45, 121.52, 126.92, 126.99, 128.76, 129.86, 142.13, 162.05, 164.39, 164.52. FT-IR (KBr) (cm^{-1}): 3200, 3011, 2926, 2856, 1668, 1629, 1607, 1541, 1500, 1471, 1256, 1174, 840, 748 cm^{-1}; MS (20 eV EI) *m/z* (*I* %): 393 (53.40) $[M]^+$. HRMS Calcd for $C_{25}H_{32}N_2O_2$: 392.2463; Found: 392.2463. Elemental analyses: calculated for C: 76.49, H: 8.22, N: 7.14; found C: 76.49, H: 8.11, N: 7.11.

*5.2.4 Synthesis of **3a–3b**.*

Compound **1a** (1 mmol), the corresponding *para*-substituted benzyl boronic acid (1 mmol), $KF{\cdot}2H_2O$ (10 mmol), and $Pd(OAc)_2$ (4 μmol) were mixed and put into a 10 ml test tube, which was placed into a household microwave oven (Glanz WP800TL23-KL, 800W) for about 30 seconds. When the mixture turned into a brown liquid, the reaction was complete and the microwave irradiation was stopped immediately. The test tube was removed from the microwave oven after the reaction mixture had been cooled to room temperature. The crude product was dissolved in $CHCl_3$ and was purified by silica gel column chromatography using CH_2Cl_2/ethyl acetate mixture (v/v=25:1) as an eluent to afford the reaction products **3a–3b** as off-white solids. Yields: 39–48%.

2-(4′-Chloro-4-biphenyl)-5-(4-decyloxyphenyl)-1,3,4-thiadiazole **3a**: ^{1}H-NMR ($CDCl_3$): δ (ppm)=8.02 (d, *J*=8.4 Hz, 2H), 7.95 (d, *J*=8.7 Hz, 2H), 7.68 (d, *J*=8.4 Hz, 2H), 7.58 (d, *J*=8.7 Hz, 2H), 7.45 (d, *J*=8.7 Hz, 2H), 7.00 (d, *J*=8.7 Hz, 2H), 4.03 (t, *J*=6.6 Hz, 2H), 1.84–1.80 (m, 2H), 1.55–1.23 (m, 14H), 0.89 (t, *J*=6.6 Hz, 3H). ^{13}C-{^{1}H}-NMR ($CDCl_3$): δ (ppm)=168.27, 166.98, 161.81, 142.56, 138.52, 134.37, 129.64 129.30, 129.00, 128.50, 128.22, 127.75, 122.63, 115.25, 68.47, 32.05, 29.71, 29.53, 29.47, 29.30, 26.15, 22.83, 14.26. MS (20 eV EI) *m/z* (*I* %): 505 (58.78) $[M]^+$. HRMS Calcd for $C_{30}H_{33}ClN_2OS$: 504.2002; Found: 504.2002. Elemental analyses (%): calculated for C: 71.33, H: 6.59, N: 5.55; found C: 71.35, H: 6.29, N: 5.46. FT-IR (KBr) (cm^{-1}): 2919.9, 2851.2, 1602.2, 1516.9, 1485.3, 1467.5, 1444.4, 1395.2, 1304.6, 1260.4, 1178.6, 1096.4, 1020.0, 815.6, 725.7.

2-(4′-Fluoro-4-biphenyl)-5-(4-decyloxyphenyl)-1,3,4-thiadiazole **3b**: ^{1}H-NMR ($CDCl_3$): δ (ppm)=8.19 (d, *J*=8.4 Hz, 2H), 8.08 (d, *J*=9.0 Hz, 2H), 7.70 (d, *J*=8.4 Hz, 2H), 7.64–7.59 (m, 2H), 7.17 (t, *J*=8.7 Hz, 2H), 7.03 (d, *J*=9.0 Hz, 2H), 4.04 (t, *J*=6.6 Hz, 2H), 1.87–1.70 (m, 2H), 1.55–1.21 (m, 14H), 0.89 (t, *J*=6.6 Hz, 3H). ^{13}C-{^{1}H}-NMR ($CDCl_3$): δ (ppm)= 168.13, 166.97, 164.67, 161.62 (d, J_{C-F}=11.0 Hz), 142.77, 136.23, 129.62, 129.40, 128.88 (d, J_{C-F}=3.2 Hz), 128.46, 127.74, 122.75, 116.05 (d, J_{C-F}=8.6 Hz), 115.22, 68.46, 32.05, 29.71, 29.53, 29.47, 29.30, 26.16, 22.83, 14.27. MS (20 eV EI) *m/z* (I %): 489 (62.85) $[M]^+$. HRMS Calcd for $C_{30}H_{33}ClFN_2OS$: 488.2297; Found: 488.2297. Elemental analysis (%): calculated for C: 73.74, H: 6.81, N: 5.73; found C: 73.60, H: 6.59, N: 6.00. FT-IR (KBr) (cm^{-1}): 2920.0, 2850.1, 1604.5, 1519.0, 1501.4, 1467.8, 1400.7, 1304.4, 1264.5, 1236.9, 1175.9, 1159.9, 1088.2, 1023.1, 987.3, 823.8, 729.1.

*5.2.5 Synthesis of **4a–4b**.*

To a round bottom flask (100 ml) were added **2a** (1 mmol), *p*-substituted boronic acid (1 mmol), K_2CO_3 (5 mmol) and $Pd(OAc)_2$ (2 μmol) as a catalyst in a solution mixture of dioxane (30 ml) and water (10 ml) refluxed for 1 hr under nitrogen. The reaction mixture was evaporated *in vacuo*, then the solid residue was extracted by CH_2Cl_2 twice (2 × 50 ml), then dried with anhydrous $MgSO_4$, filtered and concentrated at reduced pressure. The crude product was purified by silica gel column chromatography using CH_2Cl_2/ethyl acetate mixture (v/v=15:1) as an eluent. Yields: 83–90%.

2-(4′-Chloro-4-biphenyl)-5-(4-decyloxyphenyl)-1,3,4-oxadiazole **4a**: ^{1}H-NMR ($CDCl_3$): δ (ppm)=8.19 (d, *J*=8.4 Hz, 2H), 8.08 (d, *J*=8.7 Hz, 2H), 7.71 (d, *J*=8.4 Hz, 2H), 7.58 (d, *J*=8.4 Hz, 2H), 7.45 (d, *J*=8.4 Hz, 2H), 7.03 (d, *J*=8.7 Hz, 2H), 4.04 (t, *J*=6.6 Hz, 2H), 1.87–1.78 (m, 2H), 1.55–1.21 (m, 14H), 0.89 (t, *J*=6.6 Hz, 3H). ^{13}C-{^{1}H}-NMR ($CDCl_3$): δ (ppm)=164.83, 163.99, 162.19, 143.07, 138.45, 134.49, 129.31, 128.85, 128.53, 127.64, 127.50, 123.36, 116.26, 115.16, 68.47, 32.05, 29.72, 29.53, 29.47, 29.29, 26.16, 22.84, 14.27. MS (20 eV EI) *m/z* (*I*%): 489 (36.39) $[M]^+$. HRMS Calcd for $C_{30}H_{33}ClN_2O_2$: 488.2230; Found: 488.2230. Elemental analyses (%): calculated for C: 73.68, H: 6.80, N: 5.73; found C: 73.44, H: 6.96, N: 5.89. FT-IR (KBr) (cm^{-1}): 2922.3, 2850.4, 1612.0, 1496.6, 1470.9, 1394.8, 1253.7, 1177.7, 1099.9, 1011.3, 962.4, 836.5, 818.3, 744.4.

2-(4′-Fluoro-4-biphenyl)-5-(4-decyloxyphenyl)-1,3,4-oxadiazole **4b**: ^{1}H-NMR ($CDCl_3$): δ (ppm)=8.05 (d, *J*=8.4 Hz, 2H), 7.95 (d, *J*=8.7 Hz, 2H), 7.66 (d, *J*=8.4 Hz, 2H), 7.63–7.58 (m, 2H), 7.16 (t, *J*=8.7 Hz, 2H), 6.99 (d, *J*=9.0 Hz, 2H), 4.03 (t, *J*=6.6 Hz, 2H), 1.86–1.77 (m, 2H), 1.54–1.21 (m, 14H), 0.89 (t, *J*=6.6 Hz, 3H). ^{13}C-{^{1}H}-NMR ($CDCl_3$): δ (ppm)=164.77 (d, J_{C-F}=2.04 Hz), 164.05, 162.18, 161.45, 136.14, 128.95 (d, J_{C-F}=3.27 Hz), 128.84, 127.66, 127.47, 123.07, 116.29, 116.08 (d, J_{C-F}=8.55 Hz), 115.16, 68.47, 32.05, 29.47, 29.29, 26.16, 22.83, 14.27. MS (20 eV EI) *m/z* (*I*%): 473 (96.17) $[M]^+$. HRMS Calcd for $C_{30}H_{33}FN_2O_2$: 472.2526; Found: 472.2526. Elemental analyses (%): calculated for C: 76.24, H: 7.04, N: 5.93; found C: 76.39, H: 6.94, N: 5.92. FT-IR (KBr) (cm^{-1}): 2923.8, 2851.4, 1612.7, 1519.7, 1491.3, 1469.9, 1397.7, 1306.4, 1245.1, 1179.6, 1161.8, 1103.0, 1016.6, 828.3, 741.7.

Supplementary materials

Electronic supplementary information is available via the multimedia link on the online webpage: tabulated peak position and relative intensity of the strongest

diffraction peaks observed in the powder XRD patterns of **1a**–**1f**, **2a**–**2f**, **3a**, **3b**, **4a** and **4b**; experimental XRD pattern of solid sample of **1e** and simulated X-ray diffractograms calculated from its single crystal X-ray structure; variable temperature X-ray diffractograms recorded upon heating the solid samples of **1e**, **2a**, **2d**, **3b**, **4a** and **4b** and cooling their isotropic liquids; TGA curves for solid samples of **1b**, **1c**, **3a**, **3b**, **4a** and **4b**.

Acknowledgements

This work was financially supported by grants from the National Natural Science Foundation of China (Project No. 20772064). SSYC acknowledges the award of a research assistant professorship from The University of Hong Kong (HKU).

Notes

Crystal data for **1e**: $C_{24}H_{29}N_3O_3S$, M_r=439.57, triclinic, P-1, a=7.040(2) Å, b=8.992(3) Å, c=18.102(5) Å, α=78.75(1)°, β=81.81(1)°, γ=88.17(1)°, V=1112.3(6) Å^3, Z=2, T=133 K, ρ_{calcd}=1.312 g cm^{-3}, μ_{Mo}=1.765 mm^{-1}, F(000)=468, total number of unique reflections 5218 (R_{int}=0.041). Numbers of parameters=281, R1=0.046 and wR2 (all data)=0.1138. Crystallographic data (excluding structure factors) for the structure reported in this work have been deposited in Cambridge Crystallographic Data Center with CCDC numbers: 660493. Copies of the data can be obtained free of charge on application to CCDC, 12 Union Road, Cambridge CB2 1EZ, UK (fax: (+44) 1223–336–033; Email: deposit@ccdc.cam.ac.uk).

References

(1) Bahadur B. *Mol. Cryst. Liq. Cryst.* **1984**, *109*, 1–93.
(2) Zyryanov V.Y.; Pozhidaev E.P.; Smorgon S.L.; Andreev A.L.; Ganzke D.; Shabanov V.F.; Kompanets I.N.; Haase W. *Liq. Cryst.* **2001**, *28*, 741–748.
(3) Lüssem G.; Wendorff J.H. *Polym. Adv. Technol.* **1998**, *9*, 443–460.
(4) Dinescu L.; Maly K.E.; Lemieux R.P. *J. Mater. Chem.* **1999**, *9*, 1679–1686.
(5) Laschat S.; Baro A.; Steinke N.; Giesselmann F.; Hägele C.; Scalia G.; Judele R.; Kapatsina E.; Sauer S.; Schreivogel A.; Tosoni M. *Angew. Chem. Int. Ed.* **2007**, *46*, 4832–4887.
(6) Shikuma J.; Mori A.; Masui K.; Matsuura R.; Sekiguchci A.; Ikegami H.; Kawamoto M.; Ikeda T. *Chem. Asian J.* **2007**, *2*, 301–305.
(7) Girdziunaite D.; Tschierske C.; Novotna E.; Kresse H.; Hetzheim A. *Liq. Cryst.* **1991**, *10*, 397–407.
(8) Mochizuki H.; Hasui T.; Kawamoto M.; Shiono T.; Ikeda T.; Adachi C.; Taniguchi Y.; Shirota Y.. *Chem. Comm.* **2000**, 1923–1924.
(9) Wang C.; Batsanov A.S.; Bryce M.R.. *Chem. Commun.* **2004**, 578–579.
(10) Hughes G.; Kreher D.; Wang C.; Batsanov A.S.; Bryce M.R. *Org. Biomol. Chem.* **2004**, *2*, 3363–3367.
(11) Cristiano R.; De O. Santos D.M.P.; Gallardo H. *Liq. Cryst.* **2005**, *32*, 7–14.
(12) Wen C.R.; Wang Y.J.; Wang H.C.; Sheu H.S.; Lee G.H.; Lai C.K. *Chem. Mater.* **2005**, *17*, 1646–1654.
(13) Kang S.; Saito Y.; Watanabe N.; Tokita M.; Takanishi Y.; Takezoe H.; Watanabe J. *J. Phys. Chem. B* **2006**, *110*, 5205–5214.
(14) Han J.; Wang J.Y.; Zhang F.Y.; Zhu L.R.; Pang M.L.; Meng J.B. *Liq. Cryst.* **2008**, *35*, 1205–1214.
(15) Madsen L.A.; Dinggemans T.J.; Nakata M.; Samulski E.T. *Phys. Rev. Lett.* **2004**, *92*, 145505/1–14505/4.
(16) Sung H.H.; Lin H.C. *Liq. Cryst.* **2004**, *31*, 831–841.
(17) Srivastava R.M.; Neves Filho R.A.W.; Schneider R.; Vieira A.A.; Gallardo H. *Liq. Cryst.* **2008**, *35*, 737–742.
(18) Cristiano R.; Ely F.; Gallardo H. *Liq. Cryst.* **2005**, *32*, 15–25.
(19) Han J.; Chui S.S.Y.; Che C.M. *Chem. Asian J.* **2006**, *1*, 814–825.
(20) Seed A. *Chem. Soc. Rev.* **2007**, *36*, 2046–2069.
(21) Dolling K.; Zaschke H.; Schubert H. *J. Prakt Chem.* **1979**, *321*, 643–654.
(22) Dimitrova K.; Hauschild J.; Zaschke H.; Schubert H. *J. Prakt Chem.* **1980**, *322*, 933–944.
(23) Tschierske C.; Zaschke H.; Kresse H.; Mädicke A.; Demus D.; Girdziunaite D.; Bak G.Y. *Mol. Cryst. Liq. Cryst.* **1990**, *191*, 223–230.
(24) Parra M.; Hernandez S.; Alderete J.; Zúñiga C. *Liq. Cryst.* **2000**, *27*, 995–1000.
(25) Parra M.; Alderete J.; Zùñiga C.; Hernandez S. *Liq. Cryst.* **2002**, *29*, 647–652.
(26) Parra M.; Vergara J.; Zúñiga C. *Liq. Cryst.* **2004**, *31*, 1531–1537.
(27) Parra M.; Vergara J.; Zúñiga C.; Soto E.; Sierra T.; Serrano J.L. *Liq. Cryst.* **2005**, *32*, 462.
(28) Liao C.T.; Wang Y.J.; Huang C.S.; Sheu H.S.; Lee G.H.; Lai C.K. *Tetrahedron* **2007**, *63*, 12437–12445.
(29) El-Barbary A.A.; Scheibye S.; Lawesson S.O.; Fritz H. *Acta Chem. Scand. Ser. B* **1980**, *34*, 597–602.
(30) Thomsen I.; Pedersen U.; Rasmussen P.B.; Yde B.; Andersen T.P.; Lawesson S.O.. *Chem. Lett.* **1983**, 809–810.
(31) Nuchter M.; Ondruschka B.; Bonrath W.; Gum A. *Green Chem.* **2004**, *6*, 128–141.
(32) Kappe C.O. *Angew. Chem. Int. Ed.* **2004**, *43*, 6250–6284.
(33) Kiryanov A.A.; Sampson P.; Seed A.J. *J. Org. Chem.* **2001**, *66*, 7925–7929.
(34) Huang H.; Yu H.; Chen P.; Han J.; Meng J. *Chin. J. Org. Chem.* **2004**, *24*, 502–505.
(35) Lebrini M.; Bentiss F.; Lagrenee M. *J. Heterocyclic Chem.* **2005**, *42*, 991–994.
(36) Goddart C.J. *Heterocyclic Chem.* **1991**, *28*, 17–28.
(37) Tully W.G.; Gardner C.R.; Gillepie R.J.; Westwood W. *J. Med. Chem.* **1991**, *34*, 2060–2067.
(38) Perez M.; Bermejo J. *J. Org. Chem.* **1993**, *58*, 2628–2630.
(39) Wang Y.; Sauer D.R.; Djuric S.W. *Tetrahedron Lett.* **2006**, *47*, 105–108.
(40) Cui Z.; Yang L.; Li X.C.; Wang Z.; Yang X.L. *Chin. J. Org. Chem.* **2006**, *26*, 1647–1656.
(41) Tsvetkov A.V.; Latyshev G.V.; Lukashev N.V.; Beletskaya I.P. *Tetrahedron Lett.* **2002**, *43*, 7267–7270.
(42) Tao X.; Zhao Y.; Shen D.. *Synth. Lett.* **2004**, 359–361.

(43) Liu L.; Zhang Y.; Wang Y. *J. Org. Chem.* **2005**, *70*, 6122–6125.
(44) Villemin D.; Caillot F. *Tetrahedron Lett.* **2001**, *42*, 639–642.
(45) Zvonkova Z.V.; Khvatkina A.N. *Krist. Russ.* **1965**, *10*, 734–737.
(46) Kuznetsov V.P.; Patsenker L.D.; Lokshin A.I.; Tolmachev A.V. *Krist. Russ.* **1998**, *43*, 468–477.
(47) Kumar S. *Liquid Crystals: Experimental Study of Physical Properties and Phase Transition*; Cambridge University Press: CambridgeUK, 2001.
(48) Demus D.; Richter L. *Textures of Liquid Crystals*; Verlag Chemie: Weinhein, 1984.
(49) Dierking I. *Texture of Liquid Crystals*; WILEY-VCH Verlag, GmbH&Co. KGaA: Weinheim, 2003.
(50) Parra M.L.; Saavedra C.G.; Hidalgo P.I.; Elgueta E.Y. *Liq. Cryst.* **2008**, *35*, 55–64.
(51) Sato M.; Ishii R.; Nakashima S.; Yonetake K.; Kido J. *Liq. Cryst.* **2001**, *28*, 1211–1214.
(52) Sato M.; Notsu M.; Nakashima S. *Liq. Cryst.* **2004**, *31*, 1195–1205.
(53) Petrov V.F. *Mol. Cryst. Liq. Cryst.* **2005**, *442*, 63–92.
(54) Sarma J.A.R.P.; Desiraju G.R. *J. Am. Chem. Soc.* **1986**, *108*, 2791–2793.
(55) Pedireddi V.R.; Reddy D.S.; Goud B.S.; Craig D.C.; Rae A.D.; Desiraju G.R. *J. Chem. Soc. Pekin Trans.* **1994**, 2353–2360.
(56) Navon O.; Bernstein J.; Khodorkovsky V. *Angew. Chem. Int. Ed.* **1997**, *36*, 601–603.
(57) Gerkin R.E. *Acta Cryst.* **2000**, *C56*, 850–852.
(58) Moorthy J.N.; Natarajan R.; Mal P.; Venugopalan P. *J. Am. Chem. Soc.* **2002**, *124*, 6530–6531.
(59) Reddy C.M.; Kirchner M.T.; Gundakaram R.C.; Padmanabhan K.A.; Desiraju G.R. *Chem. Eur. J.* **2006**, *12*, 2222–2234.
(60) Dunitz J.D.; Schweizer W.B. *Chem. Eur. J.* **2006**, *12*, 6804–6815.
(61) Basavoju S.; Aitipamul S.; Desiraju G.R. *Cryst. Eng. Comm.* **2004**, *6*, 120–125.
(62) Britton D.; Cramer C.J. *Acta Cryst.* **2006**, *C62*, o307–309.
(63) Mantelingu K.; Kavitha C.V.; Rangappa K.S.; Naveen S.; Sridhar M.A.; Prasad J. *Mol. Cryst. Liq. Cryst.* **2007**, *469*, 121–129.
(64) Hori K.; Kuribayashi M.; Limuro M. *Phys. Chem. Chem. Phys.* **2000**, *2*, 2863–2868.
(65) Hori K.; Iwai Y.; Yano M.; Orihara-Furukawa R.; Tominaga Y.; Nishibori E.; Takata M.; Sakata M.; Kato K. *Bull. Chem. Soc. Jpn.* **2005**, *78*, 1223–1229.
(66) Hegmann T.; Neumann B.; Wolf R.; Tschierske C. *J. Mater. Chem.* **2005**, *15*, 1025–1034.
(67) *CrystalStructure* Version *3.7.0* Rigaku & Rigaku/MSC 2000–2005, 9009 New Trails Drive, Woodlands Texas 77381, USA.
(68) Watkin D.J.; Prout C.K.; Carruthers J.R.; Betteridge P.W. *CRYSTALS Issue 10*; Chemical Crystallography Laboratory: OxfordUK, 1996.
(69) Sheldrick G.M. *SHELXS97 and SHELXL97*; University of Goettingen: Germany, 1997.